

Article

Use of Recycled Construction and Demolition Waste (RCDW) in Geosynthetic-Reinforced Roadways: Influence of Saturation Condition on Geogrid Mechanical Properties

Gabriel R. Silvestre ¹, Mateus P. Fleury ^{2,3}, Jefferson Lins da Silva ² and Eder C. G. Santos ^{1,*}

¹ School of Civil and Environmental Engineering, Federal University of Goiás, Goiânia 74605-220, Brazil; gabriel.rsilvestre@gmail.com

² Department of Geotechnical Engineering, University of São Paulo, São Carlos 13566-590, Brazil; mateusfleury@usp.br (M.P.F.); jefferson@sc.usp.br (J.L.d.S.)

³ Mauá Institute of Technology (MIT), São Caetano do Sul 09580-900, Brazil

* Correspondence: edersantos@ufg.br; Tel.: +55-62-3209-6189

Abstract: Replacing natural aggregates in infrastructure with recycled construction and demolition waste (RCDW) works helps to meet the requirements established by sustainable development. This environmentally friendly proposal undoubtedly becomes better when it is carried out with geosynthetics, providing better technical performance and positive economic impacts. However, the chemical characteristics of RCDW may result in the degradation of the geosynthetics and, therefore, must be assessed and quantified. This study aims to assess the chemical degradation caused by RCDW for the mechanical properties of two types of polymeric geogrids (polyester and polyvinyl alcohol). The study evaluates the influence of the RCDW saturation condition in the chemical degradation and the possible synergism between the launching damage (drop height) and chemical degradation. Watertight tanks were constructed to maintain the geosynthetic reinforced layers in flooded, dry and open-to-environment conditions, simulating paved and unpaved roads. The occurrence of degradation was evaluated and quantified by reduction factors related to the properties of interest using statistical analysis. The results have shown a significant influence of chemical degradation on the geogrid characteristics (especially tensile strength and secant tensile stiffness), which increased when the specimens were subjected to prior launching process simulation. The reduction factor values reported herein encourage the combined use of these materials (geogrid and RCDW) and highlight the importance of assessing the chemical degradation for the design purposes of geosynthetic-reinforced roadways with alternative materials.

Keywords: recycled waste materials; geosynthetics; laboratory and field testing; sustainable development



Citation: Silvestre, G.R.; Fleury, M.P.; Lins da Silva, J.; Santos, E.C.G. Use of Recycled Construction and Demolition Waste (RCDW) in Geosynthetic-Reinforced Roadways: Influence of Saturation Condition on Geogrid Mechanical Properties. *Sustainability* **2023**, *15*, 9663. <https://doi.org/10.3390/su15129663>

Academic Editor: Fernanda Bessa Ferreira

Received: 1 May 2023
Revised: 7 June 2023
Accepted: 13 June 2023
Published: 16 June 2023



Copyright: © 2023 by the authors. Licensee MDPI, Basel, Switzerland. This article is an open access article distributed under the terms and conditions of the Creative Commons Attribution (CC BY) license (<https://creativecommons.org/licenses/by/4.0/>).

1. Introduction

The geosynthetic reinforced soil (GRS) technique has been adopted worldwide to construct road embankments, bridge abutments, steep slopes, and retaining walls. Since the 1980s, the durability of polymeric materials has been investigated and pointed out as one of the main issues to be considered in geosynthetic designs (limit state design approach) [1,2]. Geomembrane chemical degradation has been widely investigated, given that these materials are usually placed in contact with chemically aggressive and/or hazardous media (e.g., solid waste landfills). In contrast, although important studies have been carried out, geogrids have been less investigated on this aspect, probably due to their commonplace applications in non-aggressive environments.

In another context, various studies have investigated adopting recycled aggregates as an alternative to promote sustainable and environmentally friendly solutions for the construction industry. In geotechnical engineering, recycled construction and demolition waste (RCDW) has been investigated specifically for applications in roads, embankments,

and, more recently, as backfill materials for GRS structures. In addition to the environmental benefits pointed out from using RCDW [3–7], studies have demonstrated that RCDW has mechanical characteristics equal to or even better than natural aggregates [8–12]. These outcomes make the RCDW competitive as a raw material for the construction industry.

However, RCDW exhibits different chemical characteristics when compared with natural aggregates, which must be evaluated and considered during the design phase. Moreover, there is little information on geogrid chemical degradation caused by RCDW. To help to fill this gap, this study aims to assess the mechanical properties of geogrids after being buried in RCDW under different saturation conditions. In addition, this study investigated the synergic effect of mechanical damage (damages caused by the launching process) and chemical degradation caused by RCDW on the durability of polyester (PET) and polyvinyl alcohol (PVA) geogrids.

2. Background

A limit state design approach of GRS structures formulates the calculation of the geosynthetics' long-term-allowable tensile strength (T_a) based on the mean value of the ultimate tensile strength (T_{ult}) obtained from laboratory tensile strength tests [13–16] using Equation (1) [17,18]:

$$T_a = \frac{T_{ult}}{RF_{ID} \cdot RF_{CR} \cdot RF_{CBD}} \quad (1)$$

where RF_{ID} is the reduction factor for installation damage; RF_{CR} is the reduction factor for creep; and RF_{CBD} represents the reduction factor for chemical/microbiological degradation.

The reduction factor for installation damage (RF_{ID}) has been widely investigated using in-field tests performed with natural aggregates [19–24] and recycled aggregates [25–29]. In the same way, the reduction factor for creep (RF_{CR}) has been reported under in-isolated conditions [30–34] and in-confined conditions [35–40]. Furthermore, load calibrations and resistance factors from a reliability-based approach have been proposed for a large amount of RF_{ID} [41,42] and RF_{CR} [43] data.

Geosynthetic chemical/microbiological degradation is highly dependent on the constitutive polymer and surrounding conditions, and it is mainly caused by liquids (acids or alkalis), high temperature, oxygen presence, and microbiological and/or ultraviolet exposure, called “degradation agents”. Liquids promote changes in the polymer structure (rupture caused by the decrease in the attraction force between the molecules and by hydrolysis) and the extraction of geosynthetic additives [44]. The oxygen causes geosynthetic degradation through oxidation reactions that are easily inhibited by the incorporation of antioxidant additives [45]. Considering the microbiological effects, Ionescu et al. [46] affirmed that polymers are resistant to microbiological degradation, and Yoo et al. [47] highlighted the low microbiological content in backfilling materials used in geotechnical engineering. When geosynthetics are subjected to a humid environment with stable and high temperature (30 °C), the microbiological degradation tends to increase, but it has little influence for most geosynthetic applications [45]. The temperature acts as a catalytic effect accelerating degradation reactions as an oxidizing agent (since it promotes a dissociation of chemical bonding and releases free radicals) and promotes thermal contraction and dilatation of geosynthetics [48,49].

The degradation rate of geosynthetic materials depends on the type of polymer used in the manufacturing process. For example, polyvinyl chloride (PVC) geosynthetics are commonly degraded by high temperatures, liquids (hydrolysis), and ultraviolet light, whereas polyamide (PA) geosynthetics exhibit limited resistances to acids, oxidation, and liquids (hydrolysis) [50]. Polyvinyl alcohol (PVA)-based materials are known to be vulnerable to oxidation, but there is a lack of information about the other kinds of degradation of PVA geosynthetics. An investigation on PVA fibres used to reinforce cementitious matrices has shown a small reduction in fibre tensile strength after seven years of exposure to a high alkaline environment [51]. Nishiyama et al. [52] observed an increase in fibre degradation at temperatures ranging from 50 to 70 °C.

The mechanical properties (especially creep behaviour) of PET geosynthetics explain their wide use as a reinforcement element in GRS structures [53]. Thus, the durability of PET geosynthetics has gained attention over the last decades. Special attention has been addressed to its chemical degradation since the PET formation reaction (hydrolytic) is reversible in contact with water molecules [54], resulting in hydrolysis reactions. Hsuan et al. [44] pointed out that are two separate hydrolytic reactions. The first one takes place inside the fibres and is catalysed by protons attacking the ester groups releasing ester alcohol. Thus, the fibres continue to be attacked by water and oxygen that reacts with the free carbon atoms in the neighbourhood, generating acid and increasing the degradation. The second reaction occurs in the PET surface when it is in contact with alkaline liquids, promoting superficial pits and holes. These reactions occur significantly slowly at room temperature but are catalysed by higher temperatures [55], acids, and bases [54,56].

PET geotextiles and geogrids show a reduction in their mechanical characteristics as a consequence of rupturing polymeric chains in an acid environment (caused by the high concentration of H⁺ ions) and because of the superficial erosion (reduction in polymer molecular weight) in an alkaline environment [57]. Burgoyne and Merri [58] highlighted a direct relationship between the degradation rate and the number of carboxyl end groups in polymers. After a 50% reduction in the geosynthetics' ultimate tensile strengths, Jailloux et al. [54] observed a significant decrease in the degradation rate, which indicated a higher degradation rate in the amorphous region compared to the crystalline region. Furthermore, when in contact with soil in temperatures higher than 35 °C, PET geosynthetics are more prone to suffering from hydrolysis.

One must have in mind that the installation damage can increase the geosynthetic degradation rate due to the partial or total exposure of the geogrid fibres [59]. Santos et al. [25] observed that PET geogrid and polypropylene (PP) geotextiles exhumed 15 months after being mechanically damaged (simulation of installation damage) and left buried in RCDW (compaction with a lightweight roller—1.45 kN) exhibited reduction factors (1.20 and 1.64, respectively) higher than those caused solely by the compaction procedure (1.12 for PET geogrids, and 1.00 for PP geotextiles). Thus, the evaluation of the combined effects of mechanical damage (installation damage) and chemical degradation is an important aspect for GRS structure design with RCDW.

The chemical characteristics of the leachate from backfill material used in GRS structures may compromise the reinforcement material durability. Recently, RCDW materials have gained attention as an alternative backfill material. This sustainable solution avoids the quarries exploration [60] to obtain conventional high-quality aggregates and helps the management of the widespread generation of construction and demolition wastes (CDW). Technically, its higher mechanical properties (e.g., cohesion and friction angle) enhance its attraction as a backfill material [12,61–73]. The RCDW–geosynthetics interface properties have also been investigated by direct shear tests [10,11,70,74] and pullout tests [12,70,71,75]. A GRS structure constructed with an RCDW backfill material [76] proved to be stable and supported the foundation soil collapse [8,9]. In this way, the chemical characteristics of these non-conventional backfill materials are important data to establish reliable design parameters (e.g., RFD).

RCDW comprises several types of construction and demolition waste (CDW): Portland cement-based materials (e.g., concrete, mortar, and cement slurry), clay-based materials (e.g., ceramic, polished ceramic, tiles, and bricks), weathered rock, bituminous materials, fabric, glass, metal, lime, gypsum, plastic, wood, and others. This heterogeneity results in different chemical compounds present in the RCDW, such as silica dioxide (SiO₂) from cement-based materials and ceramics [77]; aluminium oxide (Al₂O₃) from ceramics, soil, feldspar, and cement [78–80]; calcium oxide (CaO) from cement binders [77]; sulphate contents leached from ceramic materials and gypsum [81,82]; and heavy metals leached from treated wood [83]. Furthermore, hydrogen sulphide (H₂S) emissions at CDW landfills were reported by some studies [84–87], which could have been caused by the reduced sulphur compounds [88] and sulphate bioconversions [86]. An in-field experimental

embankment constructed with geotextile and RCDW exhibited a lower concentration of sulphate after 24 months of exposure [82].

In terms of the pH values, several authors reported alkaline values for RCDW samples solubilized in distilled water [8,9,71,86,89]. A difference in the pH value was reported according to the material component: 11–12 for cement-based materials; 6–7 for gypsum; 4–7 for wood and cardboard; and 4.8–6.7 for soil samples [86,90–92]. However, Townsend et al. [86] pointed out that laboratory tests (usually performed with distilled water) differed from in situ conditions, such as when RCDW is exposed to acid rain. Lima and Cabral [93] reported on the acid pH value (6.62) for an RCDW sample leached by a solution similar to acid rain. The study reported by Coelho et al. [94] showed an average pH value of 6.58 (with extreme values equal to 5.77 and 7.30) for rain in the metropolitan region of Goiânia-GO (site of the in-field tests conducted in the present study).

To improve the knowledge of geogrid durability and encourage the application of alternative filling materials (this case, RCDW) in GRS structures, this study focused on evaluating geogrid strength reduction caused by the usual installation procedures, their chemical degradation due to the contact with RCDW under different saturation conditions, and the synergy between these two processes (damaged caused by the launching process and chemical degradation).

3. Materials and Methods

3.1. Recycled Construction and Demolition Waste (RCDW)

The RCDW used in this study was provided by a recycling plant located at the metropolitan region of Goiânia-GO, Brazil. The recycling plant carried out the crushing of the construction and demolition waste (CDW)—in a single process (jaw crusher)—and sieving as the main recycling procedures. The material studied was the product of the mixture of equal volumes of three recycled aggregates with different particle sizes (d): gravel A ($9.5 \text{ mm} < d < 19 \text{ mm}$), gravel B ($4.8 \text{ mm} < d < 9.5 \text{ mm}$), and sand ($d < 4.8 \text{ mm}$). The variability of the RCDW characteristics was assessed through laboratory tests of four samples—called RCDW 01 to 04—and each sample comprised materials collected at the recycling plant along the height of the storage pile (bottom, middle, and top)—obtained over a 21-day interval.

Laboratory tests were performed to evaluate the grain-size distribution; the Atterberg limits and compaction test (Standard Proctor), following the current national technical standards (Brazilian Standards—NBR) established by the Brazilian Association of Technical Standards (ABNT, in Portuguese). The hydrogen ion concentration (pH) test was performed according to the procedure stated by the United States Environmental Protection Agency (USEPA 9045D [95]). Furthermore, composition tests were performed by visual (naked eye) separation of particles retained at mesh #4 (4.78 mm)—particles passing through mesh #4 during the sieving process under running water were considered as “soil”. A detailed explanation of the composition test was reported by Santos [96], Leite et al. [97], and Fleury et al. [29].

3.2. Geosynthetics

To assess the effects of chemical degradation in different constitutive polymers, two geogrids commonly used for GRS structures in Brazil were adopted in this study. The first one (GG-PET) consisted of a high tenacity polyester (PET) yarn, with a mass per unit area (M_A) equal to 185 g/m^2 , an open size of $25 \times 25 \text{ mm}$, an ultimate tensile strength (T_{ult}) equal to 35 kN/m , and strain at failure (ϵ_f) lower than 10%. The other geogrid (GG-PVA) was made of polyvinyl alcohol (PVA) yarn coated by polyamide (PA) resin and had an M_A equal to 160 g/m^2 , an opening size of $30 \times 25 \text{ mm}$ (machine and cross-machine directions, respectively), a T_{ult} equal to 35 kN/m , and an ϵ_f lower than 6%. GG-PET and GG-PVA were chemically resistant to environments with pH values between 2–10 and 2–13, respectively, according the geosynthetic supplier. For the experimental program, geogrid meshes (1.20 m

by 1.40 m in longitudinal and transversal directions, respectively) were obtained for each geogrid from a single batch (roll) provided by the manufacturer.

3.3. In-Field Experimental Program

The experimental program was carried out using three tanks (2.82 m long, 1.20 m wide, and 1.00 m height), presented in Figure 1, constructed over a reinforced concrete layer (50 mm). The internal and external walls of the tanks were covered by polymeric grout and sealing additive. Furthermore, inside the tanks, a layer of plaster with sealing additive was applied to improve impermeable conditions. The sealing additive adopted was chosen carefully to avoid the dissolution of its chemical components to the water inside the tanks. Collecting tubes (20 mm diameter) were installed at three different heights: 270 mm (H1), 540 mm (H2), and 810 mm (H3) to allow the collection of the RCDW leachate. The tubes were installed at the right (R) and left (L) sides of each tank (see Figure 1b). Two tanks (the ones located at the facility end) were covered with roof tiles to protect the tanks from rainfall (Figure 1a), and thus allowed the controlled condition of saturation.

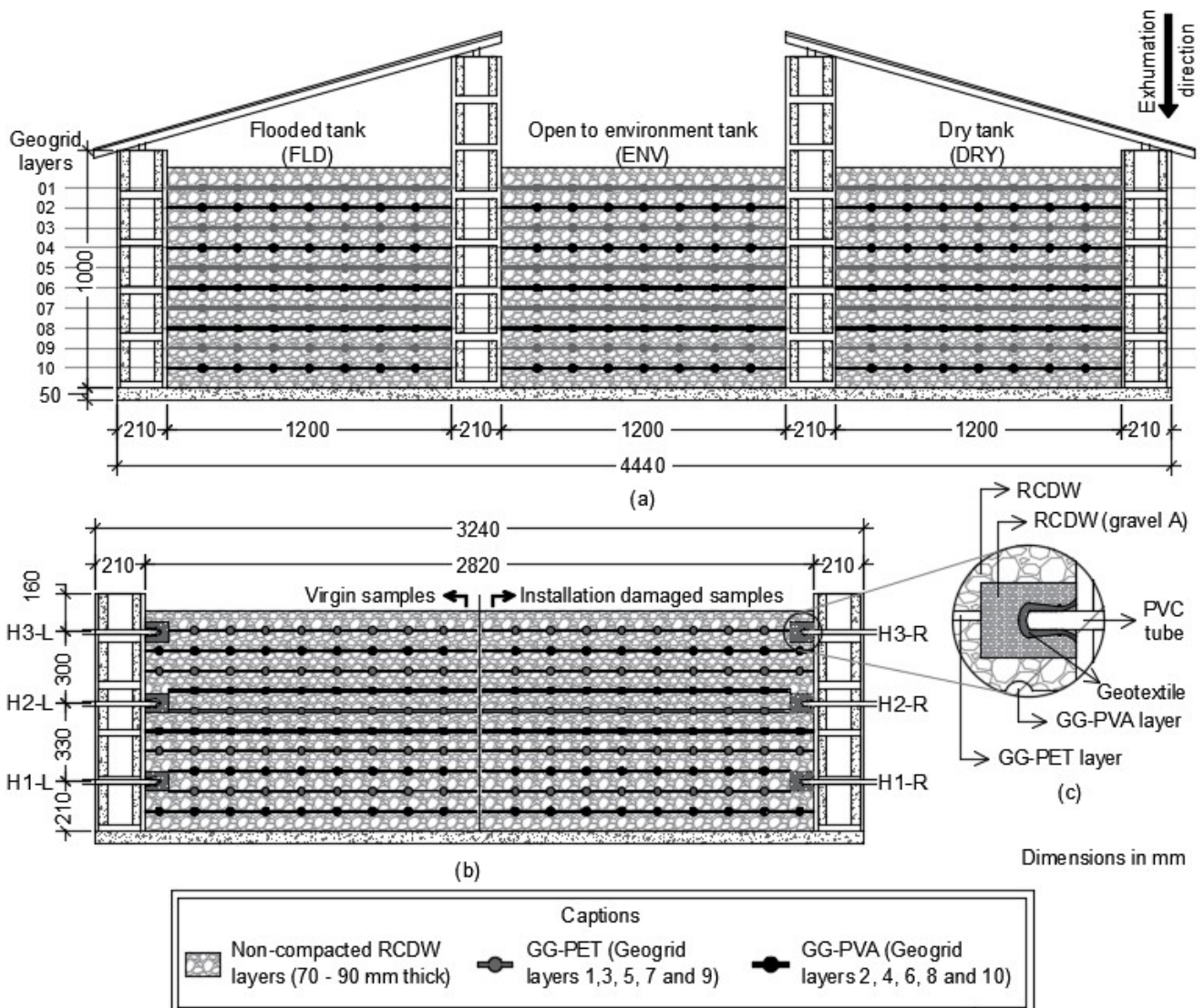


Figure 1. Illustration of the watertight tank: (a) longitudinal cross-section; (b) transversal cross-section (the same for all tanks); and (c) detail of the recycled construction and demolition waste (RCDW) leachate collector tube.

This study assessed the mechanical properties of geogrids after being buried in RCDW under two integrity conditions: (i) virgin (VS; as received from the manufacturer) and (ii) mechanically damaged (ID; after exposure to simulation of installation damage caused by the launching process). The installation damage simulation did not involve the compaction of the RCDW material. The geogrid meshes were laid over the surface, and a wooden board was arranged over them to delimit the area to be damaged. The damage consisted of dropping the RCDW (the same material used to fill the watertight tanks) from a height of 2.0 m (using a backhoe loader) over the geogrid meshes laid on the recycling plant's surface. The backhoe raised the RCDW material to a 2.0 m height, and the material was dropped over the delimited area (equal to specimen dimensions required to tensile strength test). These procedures were similar to the procedures adopted by Fleury et al. [29]. After the RCDW drop from a 2.0 m height, the geogrid meshes were exhumed using the appropriate equipment to avoid additional damages. The ribs' cut ends (longitudinal and transversal) of the virgin and damaged geogrid samples were coated with silicone to avoid contact of RCDW leachate with the geogrid yarns through these points during the immersion test in the watertight tanks.

During the tank filling process, RCDW samples were collected (samples codes RCDW FLD-0, RCDW ENV-0, and RCDW DRY-0) for control characterization. The tanks were equally filled with intercalated courses of RCDW (carefully laid and not compacted; 70–90 mm thick) and geogrid samples (VIR and ID samples of the same geogrid type were arranged side by side), which were also interleaved based on the geogrid polymer (see detail in Figure 1b). A total of ten geogrid layers (five layers for each geogrid type) was arranged avoiding contact between the geogrids and watertight tank walls. Three different saturation conditions were investigated in this experimental program (one condition per tank; Figure 1a): (i) completely flooded (FLD); (ii) open-to-environment (ENV); and (iii) dry (DRY; moisture content equal to the RCDW initial condition). Each tank was filled with RCDW material with a moisture content between 7.2% and 9.8%—values obtained from RCDW sampled during the experiment construction. The flooded condition (FLD tank) was maintained by means of level monitoring and adding water (7.29–8.36 *pH* value), avoiding the upper RCDW layer to be exposed to air. The water added to the tanks was obtained by the university's reservoir served by the local supplier system (in with the quality control system aims to provide water with a neutral *pH*). In the FLD tank, the water could solely leave by evaporation. The DRY tank condition had the adoption of roff tiles to cover its structure (as indicated in Figure 1a). The ENV tank was periodically inspected to remove undesirable material that fell into the tank.

Throughout the experimental program, climatological data (air temperature, relative humidity, and precipitation) were collected from a weather station located 150 m distant from the watertight tanks (Figure 2). The RCDW leachate was collected (when present) from all tubes (H1-L, H2-L, H3-L, H1-R, H2-R, and H3-R; Figure 1b) of each tank (FLD, ENV, and DRY) to assess its *pH* value in, approximately, 5-day intervals. Additional samples of RCDW were collected from each tank after 180-day exposure (sample codes RCDW FLD-2E, RCDW ENV-2E, and RCDW DRY-2E) to evaluate some parameters of interest.

Statistical analysis was adopted to validate the occurrence of damage and its consequent effect on the parameters of interest. The Student's *t*-distribution was used to calculate the virgin specimens' (VS) confidence intervals for the properties of interest (T_{ult} , ε_t , J_1 , and J_2), based on Equation (2).

$$X_m = \bar{X} \pm \frac{t \cdot s}{\sqrt{n}} \quad (2)$$

where X_m is the maximum or minimum value of the parameter of interest; \bar{X} is the mean value of the parameter of interest obtained by five wide-width tensile tests performed with virgin specimens (ASTM D 6637-15) [13]; t is the value of the Student's

t -distribution variable; s is the sample standard deviation; and n is the sample size (number of specimens tested).

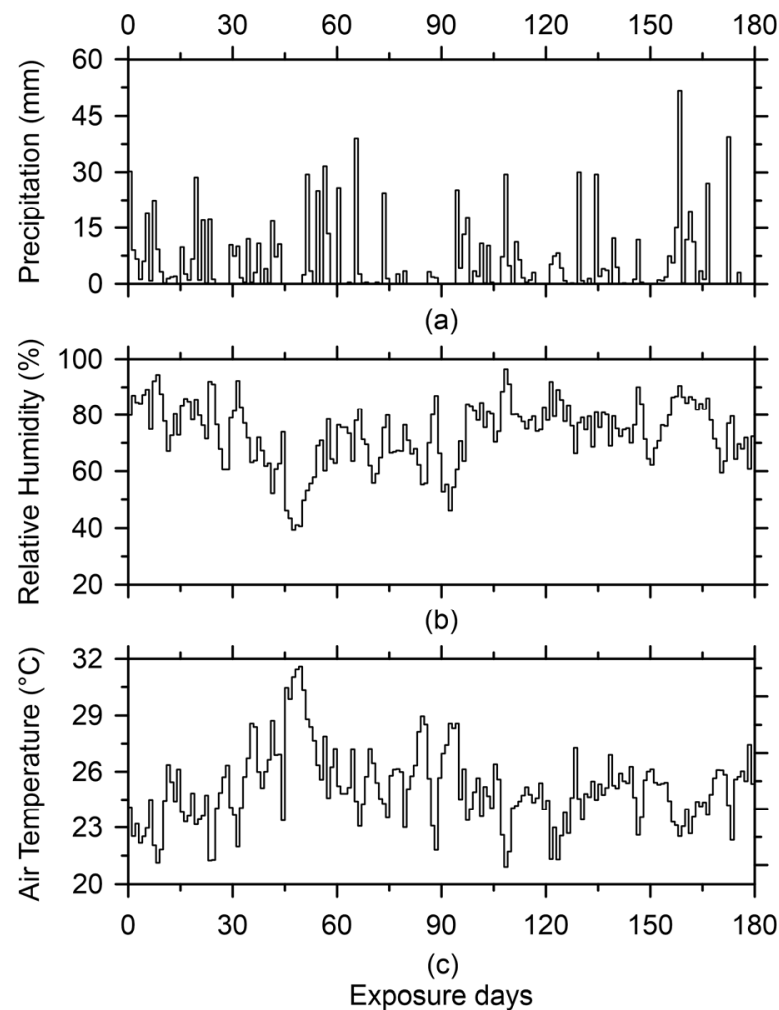


Figure 2. Climatological data obtained from a weather station located 150 m distant from the watertight tanks: (a) precipitation, (b) relative humidity, and (c) air temperature.

The confidence level used to calculate the value of t was defined in a way that all the results of all virgin specimens tested of a specific geogrid were inside the lower confidence intervals, which meant between the maximum and minimum values provided by Equation (2).

The values of the reduction factors were calculated based on the mean values of virgin and damaged and/or degraded geogrids' specimens and the confidence intervals obtained by Equation (2), as follows:

- If the mean value of a parameter of interest obtained by five wide-width tensile tests performed in damaged and/or degraded specimens fell inside the confidence intervals of the virgin specimens, the reduction factor was assumed as equal to 1.00, given that this scenario represented doubts about damage occurrence;
- On the other hand, if the mean value of a parameter of interest obtained by five wide-width tensile tests performed in damaged and/or degraded specimens fell outside the confidence intervals of the virgin specimens, the reduction factor was calculated according to Equation (3).

$$RF = \bar{X} / \bar{X}_D \quad (3)$$

where RF is the reduction factor; \bar{X} , the mean value of the parameter of interest obtained by five wide-width tensile tests performed in virgin specimens; \bar{X}_D is the mean value of the parameter of interest obtained from five wide-width tensile tests performed with damaged and/or degraded specimens; and X is the parameter of interest (T_{ult} , ε_f , J_1 or J_2).

The test methods adopted in this study possessed some limitations that must be highlighted. Firstly, the installation damage investigated did not involve the compaction of the backfill material over the geogrids. It comprised the dropping process from a 2.0 m height, considered by Fleury et al. [29] to be less aggressive than the compaction procedure. Finally, the investigation assessed the geogrids' mechanical properties (wide-width tensile tests) after a short exposure period (180 days).

4. Results and Discussion

4.1. Recycled Construction and Demolition Waste (RCDW)

4.1.1. Variability Assessment

The variability assessment was made based on the RCDW 01 to RCDW 04 test results. The composition test results (Table 1) showed that the RCDW was composed of high-quality materials and was classified as inert material—"Class A"—according to the Brazilian National Environment Council (CONAMA, in Portuguese) [98]. Results revealed the predominant soil, cementitious materials (Portland concrete and mortar), and ceramics (brick tiles and polished ceramics), in this order, which comprised more than 98% of all samples tested. Soil and cementitious materials exhibited a high variation, with a standard deviation (s) close to 14.3%; followed by the ceramic content (s equal to 2.7%). The other components showed slight variability, with s values lower than 0.5%.

Table 1. Recycled construction and demolition waste (RCDW) sample compositions in percentages by weight.

Component	RCDW 01	RCDW 02	RCDW 03	RCDW 04	RCDW FLD-0	RCDW ENV-0	RCDW DRY-0
Soil (%)	48.63	37.54	61.19	13.73	48.77	47.17	47.21
Concrete and mortar (%)	41.79	59.94	36.26	78.64	48.84	50.05	49.87
Ceramic (bricks and tiles) (%)	7.63	0.51	0.90	4.55	1.07	1.14	0.94
Polished ceramic (%)	0.50	0.17	0.15	0.92	0.17	0.20	0.27
Weathered rock (%)	0.71	1.61	1.21	0.64	0.23	0.39	0.54
Bituminous materials (%)	0.17	0.03	0.10	0.53	0.49	0.68	0.76
Others ¹ (%)	0.57	0.20	0.19	0.99	0.43	0.37	0.41

Note: ¹ Includes cardboard, fabric, glass, metal, plaster, plastic, rubber, and wood.

The grain size distribution curves indicated the presence of variability that would be better evaluated for the design of GRS structures through a grain size distribution range (RCDW range), as presented in Figure 3a. The small number of grains with dimensions between 1.0 mm and 10.0 mm in the RCDW 04 sample greatly influenced the RCDW range. In terms of the standard deviation (s) values, they were close to 15% for the particles between the abovementioned interval and equal to 5.4% for particles with a 4.8 mm diameter.

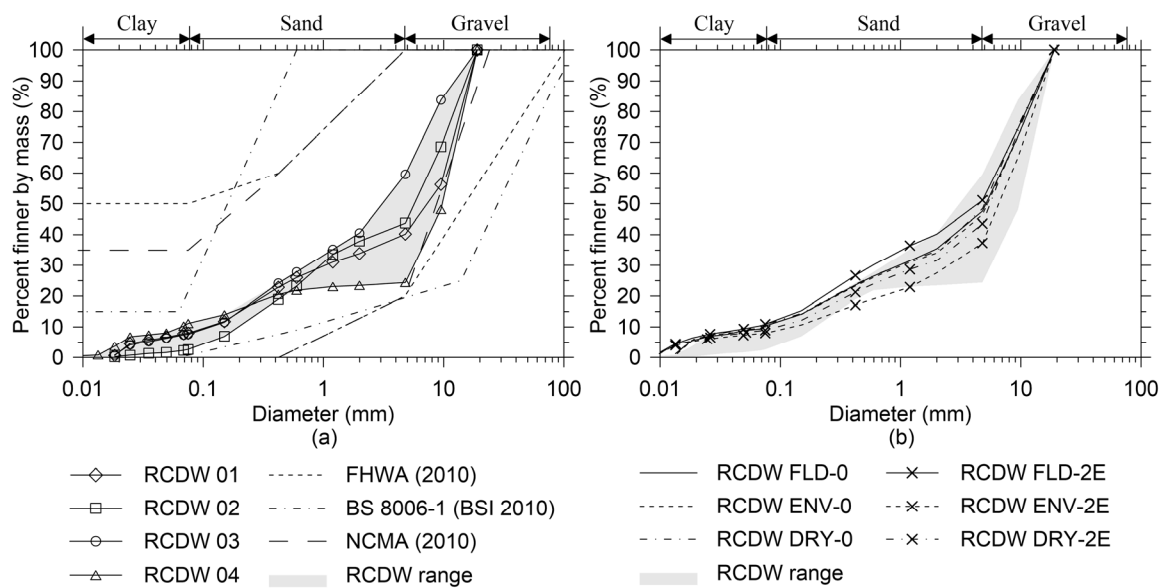


Figure 3. RCDW grain size distribution: (a) RCDW samples, RCDW grain size range, and recommendation limits for backfill material—NCMA [99], BSI [16], and FHWA [100]—and (b) RCDW samples initially used to fill the watertight tanks and after 180-day exposure (second exhumation).

No predominance was observed in soil classification for the samples according to the Unified Soil Classification System [101]. In general, RCDW classification ranged from poorly graded gravel with silt to well-graded sand with silt (Table 2), which fit EBGEO recommendations [102] for applications in GRS structures. The RCDW range was inside the backfill gradations recommended by the Federal Highway Administration (FHWA) [100], National Concrete Masonry (NCMA) [99], and the British Standard Institute (BSI) [16] for the same type of application (Figure 3a). Moreover, the non-plastic behaviour of the RCDW (Table 2) confirmed its applicability in GRS structures.

Table 2. Summary of RCDW characterisation results.

Characteristic	RCDW 01	RCDW 02	RCDW 03	RCDW 04	RCDW FLD-0	RCDW ENV-0	RCDW DRY-0
G_s	2.689	2.692	2.691	2.665	2.741	2.697	2.719
PI	NP	NP	NP	NP	NP	NP	NP
USCS	GW-GM	GW	SW-SM	GP-GM	GW-GM	GW-GM	GW-GM
$\gamma_{d,max}$ (kN/m ³)	16.96	17.38	17.42	-	18.06	17.83	17.69
w_{op} (%)	16.3	17.6	18.1	-	17.3	17.0	14.4
pH	11.50	11.60	11.77	12.03	10.64	10.00	9.67

where G_s = specific gravity of grains passing through 4.76 mm sieve; PI = plasticity index; NP = non plastic behaviour; USCS = Unified Soil Classification System (ASTM D 2487-06 [101]); GW-GM = well-graded gravel with silt; GW = well-graded gravel; SW-SM = well-graded sand with silt; GP-GM = poorly graded gravel with silt; $\gamma_{d,max}$ = maximum dry unit weight; w_{op} = optimum water content; pH = hydrogen ion concentration.

Regarding the compaction tests (Standard Proctor), sample RCDW 04 was not tested due to its low quantity of fine particles (see Figure 3a). The results of the other three samples (RCDW 01 to 03) revealed the mean value of the maximum dry unit weight ($\gamma_{d,max}$) and optimum water content (w_{op}) equal to 17.25 kN/m³ and 17.3%, respectively (Table 2). Both parameters exhibited a small variability with coefficient of variation (COV) values of 5.36% for w_{op} and 1.48% for $\gamma_{d,max}$. Similar results were reported by O'Mahony [62], Aqil et al. [64], Santos et al. [8,9,76], Vieira et al. [71], Vieira [72], and Soleimanbeiji and Likos [73].

The hydrogen ion concentration (pH) of the RCDW samples presented alkaline behaviour (Table 2) with a mean value of pH equal to 11.7 ($COV = 1.98\%$) mainly due to the presence of cementitious materials. The mean pH value was similar to other RCDW reported in the literature [89,96].

4.1.2. Materials Used in Watertight Tanks

The RCDW samples collected during the process of filling the tanks had a negligible difference between them, related to their composition (Table 1). The highest standard deviation s value was 0.91% (related to the soil content). The results showed that the tanks were filled with RCDW consisting mainly of soil and cementitious materials, a composition similar to the reference samples (RCDW 01 and 04). In terms of grain size distribution, the curves of the material used in the tanks were overlapped (highest standard deviation (s) value equal to 1.98%) and located inside the RCDW range (Figure 3b). The materials were classified as well-graded gravel with silt (GW-GM) according to the Unified Soil Classification System [101]. Moreover, the samples did not present plastic behaviour. The similarity of the material used to fill the tanks was an important aspect to make a comparison between the results (RCDW characteristics over a specified period and geogrid chemical degradation) obtained by each tank condition.

In terms of pH , the RCDW used to fill the tanks revealed a mean value equal to 10.2 ($COV = 2.68\%$). As shown in Figure 1b, PVC collector tubes were installed on the right and left sides of each tank to collect RCDW leachate and assess its pH value. Over the 180 exposure days, for each specific collector height (H1, H2, and H3), slight differences were observed between the pH values measured on both sides of the tanks. The biggest difference was observed in the flooded tank for the exposure of 70 days ($s = 0.66$; Figure 4a) in the higher collector tube (810 mm from the reinforced concrete base; H3). Thus, the assessment of the RCDW leachate pH values throughout the mean value of both sides' measurements was a reasonable consideration and is presented in Figure 4b.

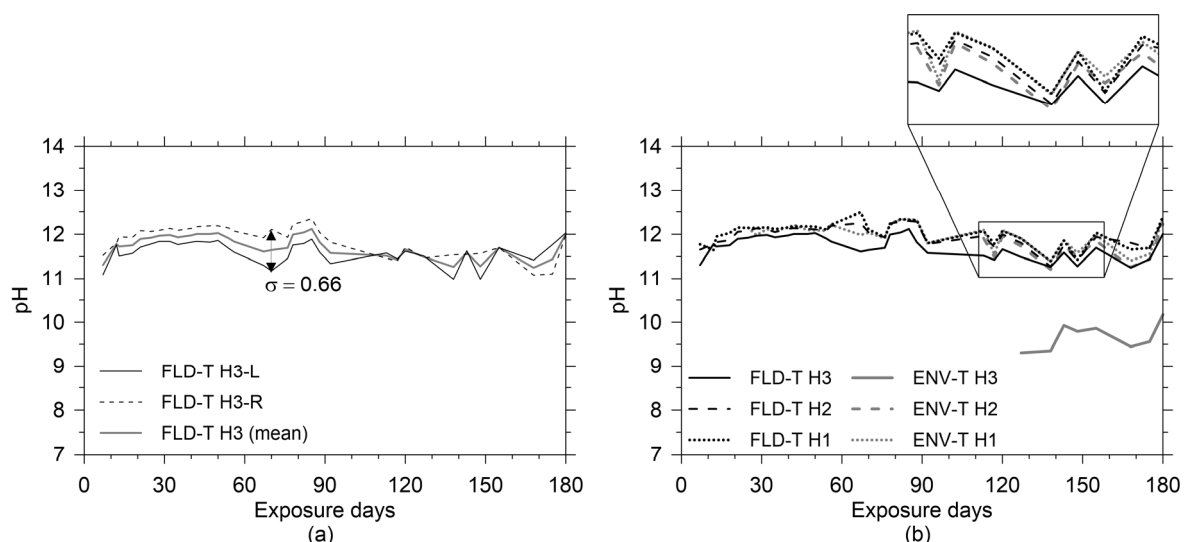


Figure 4. pH values of the RCDW leachate: (a) difference between the pH values collected from the right (R) and left (L) collector tubes located at the flooded (FLD) tank, and (b) the evolution of the pH values for the flooded (FLD) and open-to-environment (ENV) tank for the three collector tube heights.

For both tanks, the pH values of the RCDW leachate collected from tubes H1 and H2 were very similar during the analysed period. In the case of the open-to-environment tank (ENV), the first RCDW leachate started to be collected in the H1, H2, and H3 collector tubes at 25, 113, and 127 exposure days, respectively. The pH values of the RCDW leachate collected from the tubes positioned in the tanks' higher parts (H3) exhibited the smallest pH values, and those (leachate) collected from the bottom collector tube (H1) showed the

highest pH values. This indicated that the RCDW leachate pH values increased from top to bottom, i.e., in the sequence H3, H2, and H1, in both tanks (FLD and ENV). The pH values of the RCDW leachate collected from tubes H3 in the FLD and ENV tanks may have been influenced by the pH value of the water used to maintain the tank in the flooded condition and by the rain-water pH values, respectively. As expected, it was not possible to obtain RCDW leachate from the dry tank (DRY). The pH mean values of the RCDW leachate collected in the FLD tank at H1, H2, and H3 were equal to 12.03, 11.97, and 11.74, respectively. Considering the ENV tank, at H1, H2, and H3, the pH mean values were equal to 11.99, 11.67, and 9.68, respectively.

After 180 days of exposure, the basic characterisation of the RCDW samples collected indicated a slight change in the grain-size distribution curve of the material used in each watertight tank (Figure 3b). Three hypotheses could explain the difference in the grain-size distribution curves after the 180 exposure days: (i) it could have resulted from the intrinsic variability of the RCDW materials; (ii) for the case that occurred, a decrease in the particles' sizes after this period (as the RCDW material in the FLD tank experienced) it may have been caused by the disaggregation of some RCDW particles in contact with the water used to fill the tanks. In this case, the possible occurrence of suffusion, the movement of finer particles from the voids of courser particles, could not be considered since seepage force did not occur during the tests; (iii) the aggregation of soil particles may have occurred due to the dehydrated cement particles' cementation, leading to an increase in the particle diameter and a decrease in the material passing through each sieve (as experienced by the RCDW material used in the ENV tank). Possibly, the wet and dry cycles contributed to this phenomenon in the ENV tank. However, these analyses were made solely based on grain-size distribution curve changes after the 180 exposure days. Further specific investigations are required to assess these findings.

The liquid parameter analysis of the RCDW leachate of the second exhumation (Table 3) indicated that the leachate had an aluminium content higher than the limits recommended by Brazilian Association of Technical Standards (ABNT, in Portuguese) [103]. In terms of the other parameters (chloride, fluoride, iron, and alkalinity), the results were similar to the ones described by Townsend et al. [86]. According to the ABNT [103], the RCDW used in this experimental test was classified as an inert material (waste).

Table 3. RCDW leachate liquid parameters.

Parameter	NBR 10004 [103]	FLD (mg/L)	ENV (mg/L)
Alkalinity (CaCO ₃)	-	480.13	419.29
Cl ⁻	250	161.76	153.02
Fl ⁻	1.5	0.89	0.77
Al	0.2	0.32	0.36
Fe	0.3	0.15	0.16

4.2. Geogrids

4.2.1. Assessment Tensile Tests in Virgin Specimens and Determination of the Confidence Intervals

The five stress–strain curves obtained after the tensile tests performed in GG-PET and GG-PVA virgin specimens are shown in Figure 5a,b, respectively. Additionally, Table 4 summarises the mean, COV , confidence level, and the confidence interval values of the properties of interest. The smaller ultimate tensile strength (T_{ult}) values obtained compared to the information provided by the manufacturers did not impair this study since all geogrid samples and specimens were obtained from the same batch (one batch for each geogrid type). As can be seen in Figure 5, the variability (in terms of COV) of most of the properties (except T_{ult}) obtained after the tensile tests in GG-PET were higher than those from GG-PVA, which resulted in a confidence interval range (the difference between the maximum and minimum limits) wider for GG-PET (see Table 4). Damaged and/or degraded scenarios with the mean values of the parameter of interest within their

respective confidence intervals were associated with a reduction factor equal to 1.00. In fact, the variability among the virgin parameters' mean values must have been considered in the design. The confidence intervals for investigated parameters were obtained within confidence levels ranging from 96% to 98% (Table 4).

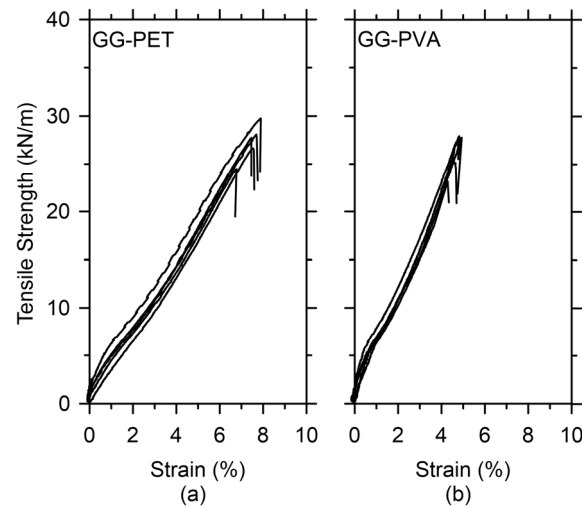


Figure 5. Tensile-strain curves of geogrids samples tested: (a) GG-PET; and (b) GG-PVA.

Table 4. Results from tensile tests (five specimens) on virgin geogrid samples associated with the Student's *t*-distribution analysis.

Characteristics	GG-PET	GG-PVA
T_{ult} (kN/m)	27.36	26.34
Coefficient of variation (%)	7.18	7.80
Confidence level (%)	97	98
Student's <i>t</i> -distribution variable	3.298	3.747
Confidence interval (kN/m)	24.46–30.26	22.90–29.78
ε_f (%)	8.70	4.66
Coefficient of variation (%)	9.16	5.39
Confidence level (%)	96	97
Student's <i>t</i> -distribution variable	2.999	3.298
Confidence interval (kN/m)	7.63–9.77	4.29–5.03
J_1 (kN/m)	520	687
Coefficient of variation (%)	12.16	8.75
Confidence level (%)	98	98
Student's <i>t</i> -distribution variable	3.747	3.747
Confidence interval (kN/m)	414–626	586–787
J_2 (kN/m)	386	550
Coefficient of variation (%)	11.78	6.68
Confidence level (%)	97	98
Student's <i>t</i> -distribution variable	3.298	3.747
Confidence interval (kN/m)	319–453	488–612

where T_{ult} = ultimate tensile strength; ε_f = strain at failure; J_1 = secant tensile stiffness at 1% strain level; J_2 = secant tensile stiffness at 2% strain level.

4.2.2. Effect of the Damaged Caused by the Launching Process

The installation damage (ID) effects caused by the launching process were evaluated comparing the results of the tensile tests performed in virgin geogrid specimens (VS) and the specimens subjected to the launching of RCDW from a 2.0 m drop height (Table 5). The simulation of the installation procedure caused changes in the damaged geogrid ultimate tensile strength mean values ($T_{ult,ID}$) that were inside the confidence interval of the virgin specimens (VS; Figure 6), resulting in a reduction factor for installation damage related to the ultimate tensile strength ($RF_{ID:T_{ult}}$) equal to 1.00 for both geogrids. Indeed, GG-PET

exhibited an increase (5.63%) in the $T_{ult,ID}$ value, whereas the GG-PVA showed a decrease of 7.21% in this parameter. Therefore, it should be mentioned that the GG-PVA geogrid was more sensitive to the damages caused by the launching process than the GG-PET, as some damaged specimens exhibited T_{ult} values lower than their virgin specimen (VS) confidence intervals (see the minimum data bar of scenario GG-PVA-ID in Figure 6).

Table 5. Mean values of tensile test (five specimens) for virgin and damaged specimens—effects of installation damage.

Scenario	T_{ult} (kN/m)	ϵ_f (%)	J_1 (kN/m)	J_2 (kN/m)
PET				
VS	27.36 (7.18)	8.70 (9.16)	520 (12.16)	386 (11.78)
ID	28.90 (7.03)	8.76 (5.68)	578 (21.59)	415 (16.67)
PVA				
VS	26.34 (7.80)	4.66 (5.39)	686 (8.75)	550 (6.68)
ID	24.44 (17.39)	4.58 (20.97)	762 (14.12)	604 (12.41)

where VS = virgin specimens; ID = installation damage; COV values are presented in parenthesis.

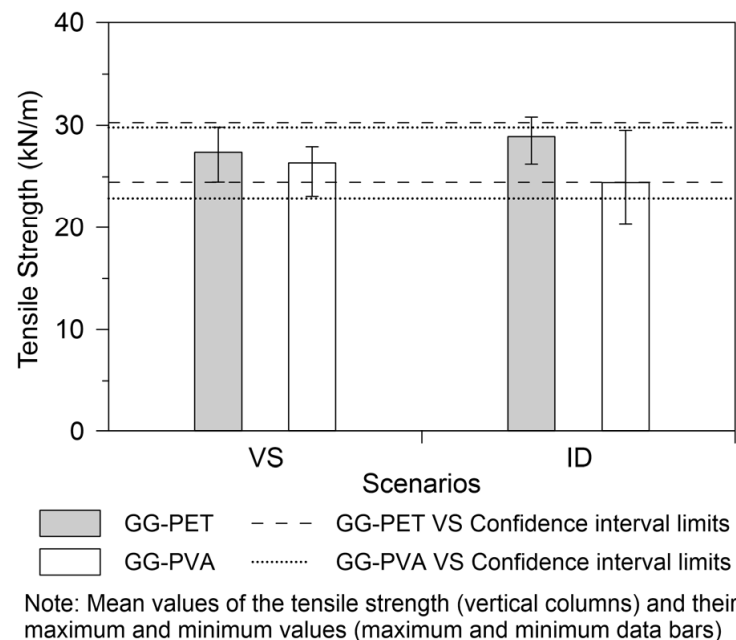


Figure 6. Effect of installation damage—launching the RCDW from 2.0 m drop height.

Regarding the strain at failure (ϵ_f), slight modifications occurred for GG-PET and GG-PVA (+0.69% and -1.72% , respectively; the negative signal represented a decrease in the value of the property compared to its virgin specimen value). All geogrids exhibited an increase higher than 7.51% of the secant tensile stiffness at 1% and 2% strains (J_1 and J_2 , respectively), but the values were within the confidence interval of the virgin specimens for these properties. The GG-PVA specimens obtained after the launching process exhibited, for all parameters of interest, COV values (in parenthesis in Table 5) higher than the ones of the virgin specimens. Thus, GG-PVA specimens exhibited values of ϵ_f , J_1 , and J_2 outside the confidence level of the virgin specimens, but the mean value of these properties fell within each parameter's confidence interval, resulting in reduction factors equal to 1.00, as shown in Table 6.

Table 6. Reduction factors for the properties of interest (all scenarios evaluated).

Scenario	T_{ult}		ε_f		J_1		J_2	
	PET	PVA	PET	PVA	PET	PVA	PET	PVA
ID	1.00	1.00	1.00	1.00	1.00	1.00	1.00	1.00
FLD-1E	1.00	1.00	1.00	0.80	1.00	1.00	1.00	1.00
ENV-1E	1.00	1.24	1.00	0.91	1.00	1.23	1.00	1.16
DRY-1E	1.00	1.18	1.00	1.00	1.00	1.00	1.00	1.13
FLD-2E	1.00	1.28	1.00	0.86	1.27	1.49	1.00	1.32
ENV-2E	1.00	1.24	1.00	0.77	1.33	1.71	1.21	1.40
DRY-2E	1.00	1.32	1.00	0.84	1.00	1.72	1.00	1.52
ID-FLD-1E	1.00	1.00	0.89	1.00	1.00	1.30	1.00	1.23
ID-ENV-1E	1.13	1.20	1.00	1.00	0.70	1.00	0.77	1.00
ID-DRY-1E	1.00	1.00	1.00	0.92	1.00	1.00	1.00	1.00
ID-FLD-2E	1.00	1.39	1.00	0.77	1.97	1.55	1.34	1.35
ID-ENV-2E	1.29	1.00	1.00	0.77	1.61	1.59	1.32	1.35
ID-DRY-2E	1.00	1.26	1.00	1.18	1.00	1.56	1.00	1.35

where PET = GG-PET (polyester geogrid); PVA = GG-PVA (polyvinyl alcohol geogrid); ID = installation damage; FLD = flooded tank; ENV = open-to-environment tank; DRY = dry tank; 1E = exhumation after 90-day exposure; 2E = exhumation after 180-day exposure.

For all properties of interest investigated herein (T_{ult} , ε_f , J_1 , and J_2), GG-PVA showed to be more sensitive to the launching process than the GG-PET. The lower flexibility of the PVA geogrid (compared to the PET geogrid) was pointed as the reason of its sensitivity. As highlighted by Fleury et al. [29], the impact energy caused by the drop height could be better distributed in flexible ribs (geogrids). It is worth to mention that flexural rigidity tests (following ASTM D 7748M-14 [104]) were not performed in the present study, but the difference in the geogrids' flexibility properties was evident during its handling.

The abovementioned results indicated that dropping the RCDW from a 2.0 m height did not cause significant changes in the geogrid properties. However, the damage caused by dropping the RCDW from a 2.0 m dropping height should not be overlooked since the investigation reported in this study evaluated backfills with continuous grain size distributions. Further investigations are required for backfill material with uniform grain size distribution since it minimizes the referred effect and enables identifying the backfill gradation in the damages caused by dropping height. In terms of reduction factors, both geogrids exhibited reduction factors equal to 1.00 regardless of the parameter investigated, as shown in Table 6.

4.2.3. Strength Reduction

The chemical degradation of the geogrids was assessed from the results (Table 7) of the tensile tests performed in virgin specimens placed in the watertight tanks and exhumed after 90 and 180 days of exposure. After 90 days of exposure, GG-PET specimens exhibited a decrease in the $T_{ult,VS}$ value (−3.8%) only in the dry tank condition (code DRY). For the other tanks, the mean ultimate tensile strength of the degraded specimens ($T_{ult,CBD}$) was slightly higher than the virgin ($T_{ult,VS}$) value (+0.15% and +0.58% for samples under flooded (FLD) and open-to-environment (ENV) conditions, respectively). Despite these differences, all $T_{ult,CBD}$ values of the GG-PET specimens fell inside its virgin confidence interval (Figure 7a), providing a reduction factor for the exhumated specimens ($RF_{CBD:T_{ult}}$) equal to 1.00 (Table 6). For the second exhumation (180-day exposure), the GG-PET samples exhibited a decrease in the virgin $T_{ult,CBD}$ values for all saturation conditions (Figure 7b). The higher reduction occurred in the DRY tank (−9.14%) followed by the ENV (−5.04%) and FLD (−2.56%). Similar to the samples tested in the first exhumation, the GG-PET $T_{ult,CBD}$ values after 180-day exposure fell within the virgin confidence interval, providing an $RF_{CBD:T_{ult}}$ equal to 1.00 (Table 6).

Table 7. Mean values of tensile test results (five specimens) for virgin and degraded specimens—effects of chemical degradation.

Scenario	T_{ult} (kN/m)	ϵ_f (%)	J_1 (kN/m)	J_2 (kN/m)
PET				
VS	27.36 (7.18)	8.70 (9.16)	520 (12.16)	386 (11.78)
FLD-1E	27.40 (7.75)	8.80 (8.15)	606 (24.96)	428 (18.74)
ENV-1E	27.52 (9.35)	8.82 (5.34)	558 (15.12)	401 (8.97)
DRY-1E	26.32 (5.64)	8.78 (7.09)	474 (28.56)	377 (13.74)
FLD-2E	26.66 (2.08)	8.90 (6.00)	410 (23.71)	352 (8.14)
ENV-2E	25.98 (7.71)	9.36 (12.01)	392 (22.34)	318 (15.27)
DRY-2E	24.86 (10.06)	8.92 (13.16)	548 (40.30)	403 (28.96)
PVA				
VS	26.34 (7.80)	4.66 (5.39)	686 (8.75)	550 (6.68)
FLD-1E	27.02 (3.46)	5.82 (10.83)	606 (13.39)	513 (13.32)
ENV-1E	21.30 (16.06)	5.10 (13.86)	560 (20.20)	476 (15.03)
DRY-1E	22.24 (5.76)	5.00 (13.93)	598 (13.88)	488 (13.83)
FLD-2E	20.52 (10.68)	5.40 (14.40)	460 (24.69)	416 (16.38)
ENV-2E	21.30 (12.58)	6.02 (20.66)	402 (18.81)	394 (13.80)
DRY-2E	19.90 (7.52)	5.52 (9.36)	400 (16.68)	361 (13.83)

where VS = virgin specimens; FLD = flooded tank; ENV = open-to-environment tank; DRY = dry tank; 1E = exhumation after 90-day exposure; 2E = exhumation after 180-day exposure; COV = values are presented in parenthesis.

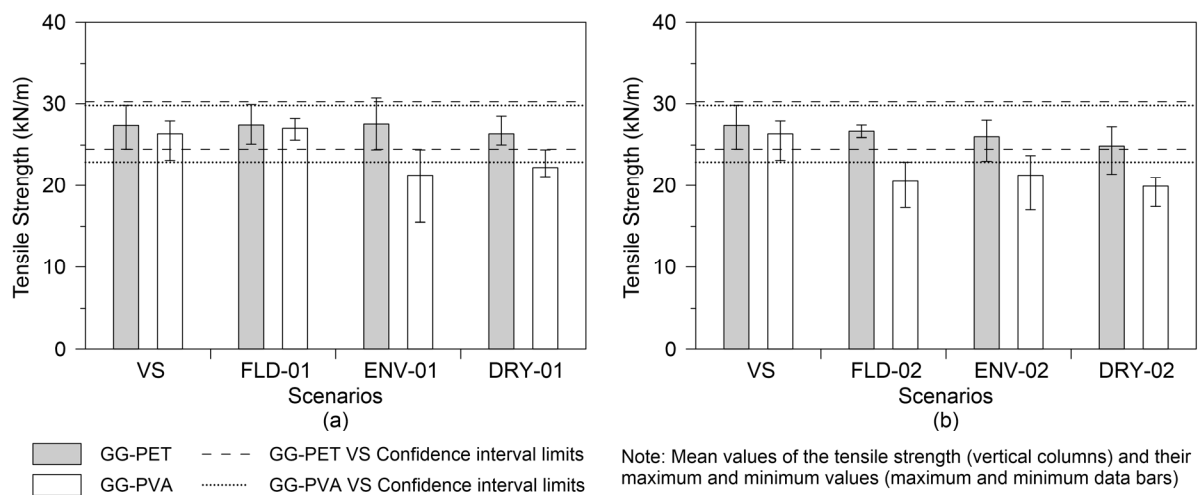


Figure 7. Effect of chemical degradation on tensile strength: (a) 90-day exposure (first exhumation—1E); and (b) 180-day exposure (second exhumation—E2).

For the GG-PVA, the 90-day exposure resulted in a reduction in the $T_{ult,CBD}$ values by -19.13% and -15.57% for the ENV and DRY tanks, respectively, resulting in $RF_{CBD:Tult}$ values equal to 1.24 and 1.18, in this order (Table 6). An increase of $+2.58\%$ compared to the $T_{ult,VS}$ value was obtained by tensile tests performed at specimens exhumed from the FLD tank—a value inside the GG-PVA virgin specimens’ confidence interval (Figure 7a; $RF_{CBD:Tult}$ 1.00). After 180-day exposure (second exhumation; Figure 7b), GG-PVA specimens from the ENV tank maintained the same level of degradation (-19.13% for the $T_{ult,CBD}$ value; $RF_{CBD:Tult} = 1.24$). The GG-PVA specimens from the FLD tank condition exhibited a reduction of -22.10% for the $T_{ult,CBD}$ value ($RF_{CBD:Tult} = 1.28$), whereas the specimens on the DRY tank condition exhibited a -24.45% reduction for the $T_{ult,CBD}$ value ($RF_{CBD:Tult} = 1.32$).

Figure 8 illustrates the evolution of the specimens’ degradation for each tank. It is evident that the GG-PET samples only buried in the FLD and ENV tanks did not suffer degradation during the first 90-day exposure, but the degradation occurred after 180-day exposure, with the specimens from the FLD tanks showing a higher degradation rate.

However, the GG-PET sample under dry conditions (code DRY) exhibited degradation since the first exhumation (90-day exposure), and its value increased by 140% during the following 90-day exposure period. On the other hand, most of the GG-PVA scenarios presented degradations for the first 90-day exposure (except for the FLD tank). However, the degradation rate between the 90th and 180th days of exposure was higher for the GG-PVA specimens under the FLD tank condition than in the other tanks (codes ENV and DRY). The degradation that was not evident in the specimen from the FLD tank in the first exhumation (90-day exposure) rapidly increased to 22.10% during the second 90-day exposure period. For the ENV tank, the degradation value did not change (negligible decrease occurs) during the following 90-day exposure period, probably because of the more stable environmental conditions (relative humidity and air temperature in the second 90 exposure days—see Figure 4b,c).

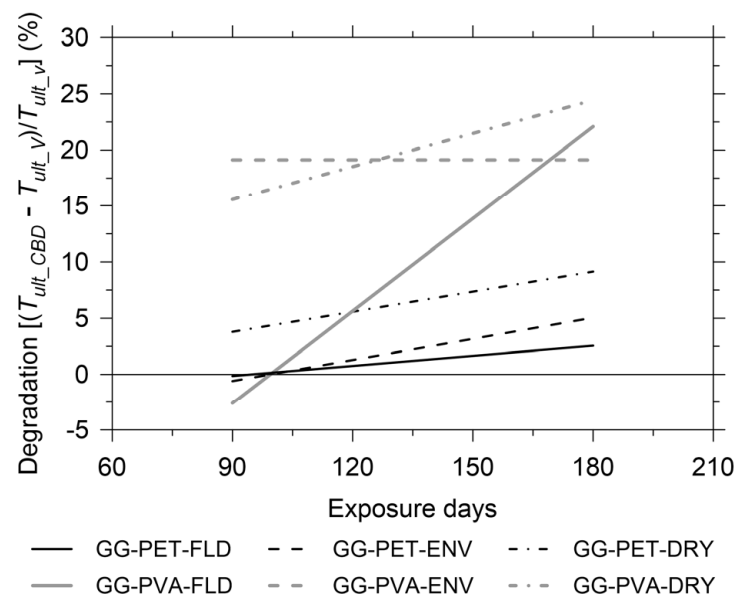


Figure 8. Evolution of ultimate tensile strength reduction due to chemical degradation under flooded (FLD), dry (DRY), and open-to-environment (ENV) conditions.

The abovementioned results indicated for the T_{ult} values that the polyester geogrid was more sensitive to degradation at dry conditions, whereas the polyvinyl alcohol geogrid was more sensitive to degradation in a flooded condition compared to a dry condition. Moreover, it was evident that the GG-PVA was more prone to degradation caused by RCDW than the GG-PET, regardless of the condition investigated.

Regarding the strain at failure (ϵ_f), both geogrids (GG-PET and GG-PVA) exhibited an increase in ϵ_f values for all conditions (FLD, ENV, and DRY), regardless of the exposure period (90- or 180-day exposure). For the GG-PET, the values of ϵ_f obtained after tensile tests in the degraded buried specimens fell within its virgin confidence interval, leading to reduction factors for chemical degradation related to the strain at failure ($RF_{CBD:\epsilon_f}$) equal to 1.00 for all investigated conditions and exposure times (Table 6). In terms of GG-PVA, all tank conditions and exposure times provided significant increases in the GG-PVA virgin buried specimens ϵ_f mean values outside the GG-PVA confidence interval for this parameter (except the specimens under 90-day exposure in the dry tank—scenario DRY-1E).

Surprisingly, the ϵ_f values of GG-PET and GG-PVA degraded specimens increased as the exposure time increased (except for the GG-PVA installed in the FLD tank). For the ENV and DRY tanks, the GG-PVA specimens exhibited a higher increase in the ϵ_f values for both exposure periods compared to the GG-PET specimens. For the first exhumation (90-day exposure), the increases in GG-PET virgin buried ϵ_f values were equal to +1.15% (FLD), +1.38% (ENV), and +0.92% (DRY), whereas the increases in the GG-PVA virgin buried ϵ_f

values were equal to +24.89% (FLD), +9.44% (ENV), and +7.30% (DRY). For the second exhumation (180-day exposure), the degraded GG-PET specimens exhibited increases of +2.30%, +7.59%, and +2.53% compared to the virgin specimen ε_f values for the tanks FLD, ENV, and DRY, in this order. For the buried GG-PVA specimens, the increases were equal to +15.88%, +29.18%, and +18.45, respectively, for the FLD, ENV, and DRY tanks. Regarding this property, both geogrids showed to be more susceptible to change (degradation) in the open to environmental condition (ENV tank), which meant the rainwater was more aggressive than the water used to maintain the FLD tank in the flooded tank condition.

The reduction factors related to elongation at failure ($RF_{CBD:\varepsilon_f}$) are shown in Table 6. The GG-PVA showed various scenarios with the reduction factor for chemical degradation related to the strain at failure ($RF_{CBD:\varepsilon_f}$) smaller than 1.00 that could not be considered/adopted in the design. Although the GG-PET geogrid did not exhibit an $RF_{CBD:\varepsilon_f}$ smaller than 1.00, it was noticed that its strain at failure increased as the exposure time increased. In fact, these results indicated that the changes in the geogrids as a result of their former polymers caused an increase in the polymeric chains, leading to an increase in the strain at failure. As the allowable deformation of GRS structures is a design concern, further investigations are required to validate this assumption, especially in terms of the creep behaviour of geogrid samples left buried in RCDW. It should be mentioned that this investigation was not within the scope of the present study.

The GG-PET specimens submitted to the three saturation conditions investigated (FLD, ENV, and DRY) did not exhibit changes in the secant tensile stiffness at 1% and 2% strain (J_1 and J_2 , respectively) outside the virgin samples' confidence interval after 90-day exposure (first exhumation)—reduction factors for chemical degradation related to J_1 ($RF_{CBD:J_1}$) and J_2 ($RF_{CBD:J_2}$) were equal to 1.00. However, for the second exhumation, GG-PET specimens buried in the FLD tank exhibited a −21.15% reduction in the virgin buried samples for J_1 , which resulted in an $RF_{CBD:J_1}$ equal to 1.27. The GG-PET secant tensile stiffness was more affected by the tank in open to environmental conditions (ENV), showing a reductions of −24.62% (J_1) and −17.62% (J_2), compared to the virgin GG-PET specimens, resulting in $RF_{CBD:J_1} = 1.33$ and $RF_{CBD:J_2} = 1.21$. GG-PET specimens buried in the DRY tank showed an increase in J_1 and J_2 values, but inside the virgin GG-PET specimen confidence intervals ($RF_{CBD:J_1} = 1.00$; $RF_{CBD:J_2} = 1.00$).

Different from GG-PET, the GG-PVA buried specimens showed significant reductions in the values of J_1 and J_2 since the first exhumation (90-day exposure). A reduction in the J_1 buried virgin value close to −12.30% was experienced by the GG-PVA specimens from the FLD and DRY tanks after the first exhumation, but the J_1 values for buried specimens fell inside the GG-PVA confidence interval leading to $RF_{CBD:J_1}$ equal to 1.00. A reduction of −18.43% ($RF_{D:J_1} = 1.23$) was experienced by the buried GG-PVA specimens after 90-day exposure in the ENV tank. For the second exhumation, a significant reduction in the J_1 was noticed for all the tanks that resulted in high $RF_{D:J_1}$ values: 1.49 (FLD), 1.71 (ENV), and 1.72 (DRY). In terms of the J_2 values, only the GG-PVA buried specimens after 90-day exposure in the FLD tank exhibited a reduction in J_2 inside the virgin confidence interval. GG-PVA specimens under 90-day exposure exhibited reductions in J_2 equal to −13.45% ($RF_{CBD:J_2} = 1.16$) and 11.27% ($RF_{CBD:J_2} = 1.13$) for the ENV and DRY tanks, respectively. After the 180-day exposure, the reduction in the J_2 buried virgin value was higher than in the J_1 buried virgin value for all tanks, leading to $RF_{CBD:J_2}$ values equal to 1.32 (FLD), 1.40 (ENV), and 1.52 (DRY).

From the four parameters of interest evaluated in this study (T_{ult} , ε_f , J_1 , and J_2), the J_1 and J_2 parameters proved to be the most affected by the contact with the RCDW in the three saturation conditions evaluated in this study. The GG-PVA showed to be more affected than the GG-PET. As expected, due to hydrolysis, the GG-PET exhibited a higher degradation of J_1 and J_2 when in contact with water (FLD and ENV tanks). After 90 exposure days, the J_1 and J_2 values were inside their respective virgin confidence intervals, but significant decreases in the J_1 and J_2 values occurred after 180 exposure days in the ENV and FLD tanks. Possibly, a degradation that affected the secant tensile stiffness had begun between

90 and 180 exposure days. On the other hand, the GG-PVA specimens exhibited higher reductions in J_1 and J_2 values under the dry tank condition (DRY). Furthermore, for both geogrids, the rainwater (ENV tank) proved to be more aggressive than the water used to maintain the flooded condition (code FLD). This result was mainly caused by the acid pH values of the rainwater of the region (6.58 pH value) [93] compared to the pH value of the water used to maintain the flooded condition (7.29–8.36 pH value).

The difference caused in the secant tensile stiffness of the geogrid may have occurred due to differences in the strain under loading. As the values of J_1 and J_2 decreased for the same strain (elongation) level, the buried specimens exhibited smaller tensile strengths than the virgin specimens. This result supported the abovementioned assumption that chemical degradation affected the deformation of the geogrids and, consequently, their polymer chains.

4.2.4. Synergism Effects

The combined effect of mechanical damage (simulation of the dropping the RCDW from a 2.0 m dropping height) and chemical degradation (contact of the geogrids with RCDW in different saturation conditions) was assessed by the results of the tensile tests performed in buried samples that were subjected to mechanical damage prior to their installation in the watertight tanks (Table 8). After 90-day exposure, the GG-PET samples buried in the FLD and DRY tanks showed slight modifications compared to the virgin geogrids' ultimate tensile strengths ($T_{ult VS}$), with values falling inside their virgin confidence interval (Figure 9). A reduction factor for synergy effects related to the ultimate tensile strength ($RF_{ID+CBD:Tult}$) was equal to 1.00. GG-PET specimens in the ENV tank presented reductions of -11.70% in the $T_{ult VS}$ value ($RF_{ID+CBD:Tult} = 1.13$) for the first exhumation (90-day exposure) and severe after the 180-day exposure (second exhumation) with a reduction of -22.73% ($RF_{ID+CBD:Tult} = 1.29$). Similar reductions in the FLD (-6.43%) and DRY (-4.70%) tanks were experienced by the GG-PET specimens after 180-day exposure that culminated in $RF_{ID+CBD:Tult}$ values equal to 1.00 for both scenarios (Figure 9). The reduction factors are summarized in Table 6.

Table 8. Mean values of tensile test results (five specimens) for virgin and degraded installation damage specimens—synergism effects.

Scenario	T_{ult} (kN/m)	ϵ_f (%)	J_1 (kN/m)	J_2 (kN/m)
PET				
VS	27.36 (7.18)	8.70 (9.16)	520 (12.16)	386 (11.78)
FLD-1E	27.70 (6.71)	9.78 (9.30)	494 (29.11)	383 (16.45)
ENV-1E	24.16 (12.01)	8.36 (15.03)	738 (43.08)	502 (34.85)
DRY-1E	27.26 (7.23)	8.76 (12.96)	422 (50.03)	365 (21.09)
FLD-2E	25.60 (4.16)	9.12 (11.77)	264 (68.95)	289 (29.24)
ENV-2E	21.14 (17.39)	9.22 (9.92)	322 (46.03)	292 (20.06)
DRY-2E	26.08 (5.44)	9.55 (15.50)	503 (23.79)	371 (17.08)
PVA				
VS	26.34 (7.80)	4.66 (5.39)	686 (8.75)	550 (6.68)
FLD-1E	25.32 (6.25)	4.84 (20.74)	688 (6.37)	447 (15.16)
ENV-1E	21.86 (8.63)	5.04 (8.94)	672 (17.59)	551 (4.32)
DRY-1E	24.52 (5.24)	6.04 (15.42)	442 (11.24)	545 (12.51)
FLD-2E	18.92 (8.40)	6.06 (11.53)	432 (15.99)	407 (5.93)
ENV-2E	23.14 (13.45)	3.96 (34.19)	440 (14.73)	408 (11.77)
DRY-2E	20.84 (10.09)	4.84 (20.74)	528 (19.52)	408 (10.38)

where VS = virgin specimens; FLD = flooded tank; ENV = open-to-environment tank; DRY = dry tank; 1E = exhumation after 90-day exposure; 2E = exhumation after 180-day exposure; COV = values are presented in parenthesis.

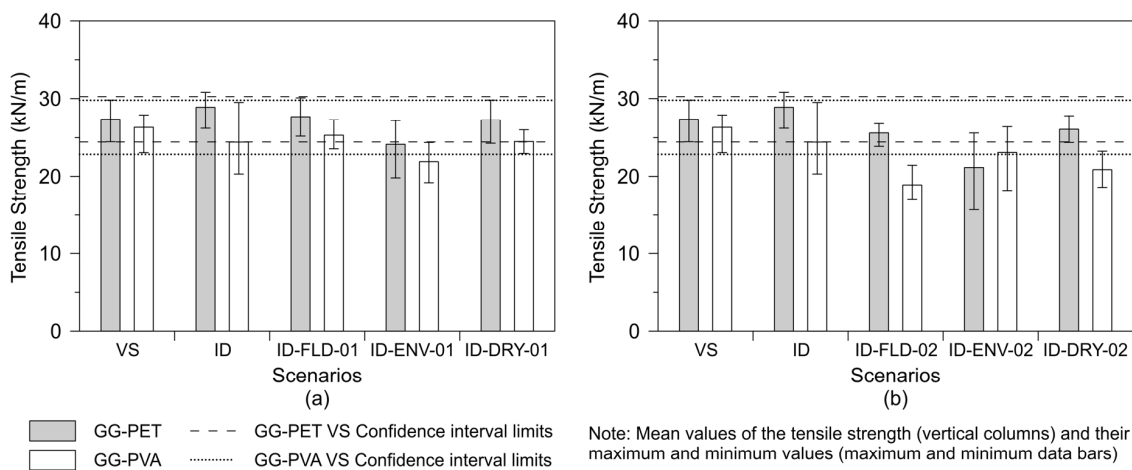


Figure 9. The synergy between mechanical damage and chemical degradation: (a) 90-day exposure (first exhumation) and (b) 180-day exposure (second exhumation).

Once again, all specimens of GG-PVA exhibited a reduction in the ultimate tensile strength values for all conditions and exposure periods. Similar to the GG-PET specimens, after the first exhumation (90-day exposure), the GG-PVA specimens presented small reductions in the $T_{ult\ VS}$ value in the FLD (−3.87%) and DRY (−6.91%) tanks, which fell inside their virgin sample confidence interval (Figure 9; $RF_{ID+CBD:T_{ult}} = 1.00$). A reduction of −17.01% in the $T_{ult\ VS}$ value was experienced by the GG-PVA samples exposed to the ENV tank, which resulted in a $RF_{ID+CBD:T_{ult}}$ equal to 1.20. In contrast to the degradation that occurred in the 90-day exposure, for the 180-day exposure, the specimens exhumed from the ENV tank exhibited a reduction (−12.15%) falling inside the GG-PVA specimens' confidence intervals. Meanwhile, the reductions experienced by the GG-PVA in the FLD and DRY tanks were equal to −28.17% ($RF_{ID+CBD:T_{ult}} = 1.39$) and −20.88% ($RF_{ID+CBD:T_{ult}} = 1.26$), respectively.

Regarding the evolution of the strength reduction (Figure 10), quite similar degradation rates were observed for the GG-PET specimens in all the conditions investigated (tanks). However, the specimens in the open-to-environment condition (ENV) exhibited the highest degradation value after 90-day exposure, which almost duplicated for the following 90-day exposure period. These results emphasised that the polyester geogrid was more sensitive to degradation in contact with rainwater than in flooded and dry conditions. Although the mechanical damage did not cause an immediate reduction in the GG-PET's ultimate tensile strength, this mechanical damage led to the exposure of the geogrid's yarns, thus accelerating the degradation process in the open to environment condition. Furthermore, it was evident that the synergic effect resulted in higher degradation rates for the PET geogrid specimens exposed to flooded and open-to-environment conditions than those related solely to the contact with RCDW (without mechanical damage—see Figures 8 and 10).

For the GG-PVA, a peculiar behaviour (a negative degradation rate) was observed for the samples exposed in the ENV tank. This unexpected result could have been associated with a non-uniform degradation of the GG-PVA specimens after 180 exposure days. As the degradation occurred due to the water (rainfall) infiltration in the tank, it may not have reached the whole area; consequently, some specimens contacted with the degradation agent (resulting in lower T_{ult} compared to the virgin specimens), and the another did not—which explained the high variability in this scenario T_{ult} value (see Table 8 and Figure 9). Despite the similar reduction values, after 90-day exposure experienced by the GG-PVA specimens in the FLD and DRY tanks, the degradation rate for the FLD tank was higher than in the DRY tank. In addition, the synergism effects in these tanks (FLD and DRY) were higher than in the specimens solely subjected to degradation (without mechanical damage). This behaviour also resulted from the fact that the launching process exposed the PVA fibres to degradation.

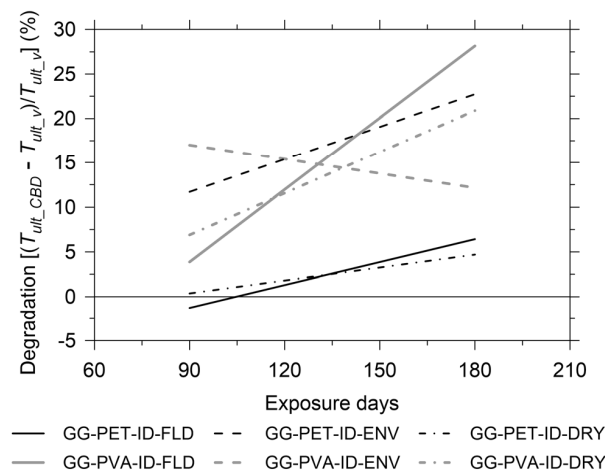


Figure 10. Evolution of the ultimate tensile strength reduction due to the synergic effects (mechanical damage and chemical degradation) under flooded (FLD), dry (DRY), and open-to-environment (ENV) conditions.

In terms of reduction factors, the simple multiplication of the reduction factors for installation damage caused by the launching process (RF_{ID}) and chemical degradation (RF_{CBD}) underestimated the combined reduction factor (RF_{ID+CBD}) for GG-PET specimens in the ENV tank (that means $RF_{ID+CBD} > RF_{ID} \cdot RF_{CBD}$). For the GG-PVA, an opposite behaviour ($RF_{ID+CBD} < RF_{ID} \cdot RF_{CBD}$) was evident for specimens from the ENV and DRY tanks. For the flooded tank, GG-PVA specimens exhumed after 180-day exposure exhibited $RF_{ID+CBD} > RF_{ID} \cdot RF_{CBD}$. The values of the reduction factors are presented in Table 6.

The strain at the failure (ϵ_f) of the specimens subjected to the combined effect of the launching process and chemical degradation exhibited similar behaviour to the specimens only subjected to the chemical degradation: an increase in the ϵ_f value as the exposure time increased was evident for most of scenarios investigated (except for scenario GG-PET-FLD, GG-PVA-ENV, and GG-PVA-DRY). However, for GG-PET specimens, the ϵ_f values after the synergic effect were maintained inside the confidence interval of the virgin specimens (except for scenario ID-FLD-1E, which exhibited a 12.41% increase compared to virgin ϵ_f values). The GG-PVA exhibited ϵ_f values inside the virgin confidence interval for samples subjected to the FLD and ENV tanks after 90-day exposure. After 180-day exposure, the ϵ_f values drastically increased ($\sim 30\%$) for both tanks (FLD and ENV). For the dry condition, the GG-PVA specimens exhibited a -8.15% reduction in the first exhumation and a 15.02% increase outside the virgin ϵ_f values in the second one.

These results highlighted that the chemical degradation process affected the stress–strain behaviour of the geogrids, especially the elongation under loading. However, in general, the synergic effect did not cause a further increase in the strains developed by the geogrids under loading compared to the ones caused solely by chemical degradation. In terms of reduction factors (Table 6), most of the GG-PET scenarios exhibited a reduction factor for the combined effect related to the strains at failure ($RF_{ID+CBD:\epsilon_f}$) equal to 1.00 (except ID-FLD-1E). Meanwhile, the GG-PVA showed a predominance of $RF_{ID+CBD:\epsilon_f}$ equal to or smaller than 1.00 (except ID-DRY-02).

Regarding the secant tensile stiffness at 1% (J_1) and 2% (J_2) strains, the GG-PET specimens exhibited reductions of 5.00% and 18.85% for J_1 and 0.78% and 5.44% for J_2 of the specimens subjected to 90-day exposure in the FLD and DRY tanks, respectively. These reductions were inside the virgin specimen confidence interval, resulting in a reduction factor for synergic effects related to the secant tensile stiffness at the 1% ($RF_{ID+CBD:J_1}$) and 2% strains ($RF_{ID+CBD:J_2}$) equal to 1.00. Increases in the J_1 (+41.92%) and J_2 (+30.05%) values were obtained after the tensile tests performed in specimens exhumed from the ENV tank after 90-day exposure, with a reduction factor smaller than 1.00 (see Table 6). For the second exhumation (180-day exposure), reductions outside the GG-PET virgin confidence interval

were observed in those tanks that allowed water contact (FLD and ENV). In the FLD tank, reductions of 49.23% for J_1 and 25.13% for J_2 resulted in an $RF_{ID+CBD;J1}$ equal to 1.97 and an $RF_{ID+CBD;J2}$ of 1.34. For the ENV tank, the reductions in J_1 (38.08%; $RF_{ID+CBD;J1} = 1.61$) and J_2 (24.35%; $RF_{ID+CBD;J2} = 1.32$) were smaller compared to the ones from the FLD tank. Slight reductions (smaller than 5.5%) in J_1 and J_2 were experienced by the GG-PET specimens in the DRY tank.

For the GG-PVA, slight changes in J_1 and J_2 values were observed for the specimens exhumed from the ENV and DRY tanks after 90-day exposure. However, values outside the GG-PVA virgin confidence interval were obtained for the J_1 (−23.09%) and the J_2 (−18.73%) in the FLD tank for the same exposure period. This last scenario exhibited $RF_{ID+CBD;J1}$ and $RF_{ID+CBD;J2}$ equal to 1.30 and 1.23, respectively. For the 180-day exposure, the specimens from all the tanks exhibited similar reductions for each secant tensile stiffness (J_1 and J_2) values. For J_1 values, the reduction ranged from 35.6% to 37.1% ($RF_{ID+CBD;J1}$ varying from 1.56 to 1.59; see Table 6), whereas, for J_2 , the reduction values were close to 26% ($RF_{ID+CBD;J2}$ equal to 1.35).

The synergic effects exhibited similar results compared to those caused by chemical degradation. The J_1 and J_2 were the parameters of interest most affected, and their reductions increased as the exposure time increased (for both geogrids). The GG-PET specimens also exhibited higher degradations (J_1 and J_2) when in contact with water (FLD and ENV) tanks. Controversially to the chemical degradation results, the reductions caused by the synergic effects in the FLD condition were higher than in the ENV condition. Regarding the GG-PVA results, the degradation caused by the combined effect (launching process and chemical degradation) reached a similar degradation level in all conditions investigated (FLD, ENV, and DRY) after 180-day exposure. These results indicated that the launching process in the GG-PVA specimens heightened its sensitivity to chemical degradations (especially for the J_1 and J_2 parameters).

In terms of reduction factors related to the J_1 and J_2 parameters (Table 6), the multiplication of RF_{ID} and RF_{CBD} proved to underestimate the RF_{ID+CBD} for both geogrids' specimens in a flooded condition (FLD tank), regardless of the exposure period, and for the GG-PET specimens exhumed after 180-day exposure in the ENV tank.

5. Conclusions

This study investigated the isolated and combined effects of installation damage caused by the launching process (non-compaction of the backfill) and the chemical degradation of geogrids caused by recycled construction and demolition waste (RCDW). Watertight tanks were constructed to reproduce three different saturation conditions (flooded, open-to-environment, and dry) for geogrid reinforced layers, using RCDW as a backfill material in road infrastructure works (road embankments, bridge abutments, steep slopes, and retaining walls). Isolated tensile tests were performed in damaged and/or degraded specimens exhumed after 90- and 180-day exposures from the watertight tanks. Based on the results obtained, the following conclusions can be highlighted.

- The RCDW used in this study had characteristics similar to other recycled aggregates reported in the literature. The variability of the RCDW's grain distribution does not prevent its application in geotechnical works. After being exposed for 180 days under flooded and open-to-environment conditions, the grain size distribution showed to be the most affected characteristic of the RCDW. In the flooded condition, disaggregation of some RCDW particles occurred (further investigation are required to assess if they occurred due to suffusion). In the open-to-environment condition, the wetting and drying cycles proved to be favourable to particle aggregation.
- The installation damage due to dropping the RCDW from a 2.0 m height did not cause immediate changes to the geogrids' ultimate tensile strengths, strains at failure, and secant tensile stiffnesses at 1% and 2% strains. However, the PVA geogrid exhibited some specimens with parameter values lower than the virgin sample confidence interval, indicating that the tested geogrid was more sensitive to installation damage compared

to the tested PET geogrid. As this study used a recycled aggregate with a specific grain size distribution, further investigations are necessary to evaluate the damage that could be caused by dropping materials with different grain size distributions.

- The tested PET geogrid showed to be more resistant to the chemical degradation caused by the RCDW than the tested PVA geogrid. For the ultimate tensile strength, the highest degradation and degradation rate in PET geogrid occurred for the dry condition, whereas, for the PVA geogrid, this occurred for the flooded condition. However, it was noted that the other properties of the tested geogrids (strain at failure and stiffness at 1% and 2% strains) were more affected by the rainwater due to their acid *pH* value compared to the flooded condition. The strain at failure exhibited higher values as the exposure period increased for all saturation conditions evaluated; the changes in the tensile stiffnesses (at 1% and 2% strains) resulted in significant changes. Regarding these properties, the PET geogrid was more affected in those conditions with rainwater contact, meanwhile the PVA geogrid experienced that for dry conditions.
- The combined effect of installation damage and chemical degradation—synergic effect—resulted in higher degradation rates for the geogrid ultimate tensile strength values compared to the isolated chemical degradation process. Even though no immediate reductions for the geogrids' ultimate tensile strengths were evident due to the installation damage (mechanical damage) simulations, they caused the exposure of the geogrid yarns and accelerated the chemical degradations. Furthermore, the synergic effect did not cause a further increase in the elongation at failure shown by the geogrids submitted to the installation damage simulation compared to those submitted solely to the chemical degradation (contact with the RCDW). The strain at failure, the secant tensile stiffness at 1% and 2% strain, presented higher values as the exposure period increased, which was a similar behaviour observed for the specimens solely exposed to chemical degradation.

Based on these conclusions, one must bear in mind that the use of RCDW as a backfill material of geosynthetic reinforced soil structures requires investigations related to the chemical degradation of the reinforcement elements. The chemical degradation has shown to be an important factor to be considered in design. Additionally, the combined effect of installation damage and chemical degradation must be previously assessed and quantified to provide adequate design parameters.

Author Contributions: Conceptualization, E.C.G.S. and G.R.S.; methodology, E.C.G.S. and G.R.S.; formal analysis, E.C.G.S., G.R.S. and M.P.F.; investigation, G.R.S. and M.P.F.; resources, E.C.G.S. and J.L.d.S.; writing—original draft preparation, E.C.G.S., G.R.S. and M.P.F.; writing—review and editing, E.C.G.S., G.R.S., J.L.d.S. and M.P.F.; supervision, E.C.G.S.; project administration, E.C.G.S.; funding acquisition, E.C.G.S. and J.L.d.S. All authors have read and agreed to the published version of the manuscript.

Funding: This research was funded by the National Council for Scientific and Technological Development (CNPq, grant No. 461018/2014-4).

Institutional Review Board Statement: Not applicable.

Informed Consent Statement: Not applicable.

Data Availability Statement: Not applicable.

Acknowledgments: The authors are indebted to the following institutions for the support given to this research: the Federal University of Goiás, the University of São Paulo, the National Council for Scientific and Technological Development (CNPq), the Research Support Foundation of Goiás (FAPEG), the geosynthetic manufacturer, the CDW recycling plant, and the engineering companies.

Conflicts of Interest: The authors declare no conflict of interest.

References

1. Cassidy, P.E.; Mores, M.; Kerwick, D.J.; Koeck, D.J.; Verschoor, K.L.; White, D.F. Chemical resistance of geosynthetic materials. *Geotext. Geomembr.* **1992**, *11*, 61–98. [[CrossRef](#)]
2. Koerner, R.M.; Lord, A.E.; Hsuan, Y.H. Arrhenius modeling to predict geosynthetic degradation. *Geotext. Geomembr.* **1992**, *11*, 151–183. [[CrossRef](#)]
3. Basu, D.; Misra, A.; Puppala, A.J. Sustainability and geotechnical engineering: Perspectives and review. *Can. Geotech. J.* **2015**, *52*, 96–113. [[CrossRef](#)]
4. Correia, A.G.; Winter, M.G.; Puppala, A.J. A Review of sustainable in transport infrastructure geotechnics. *Transp. Geotech.* **2016**, *7*, 21–28. [[CrossRef](#)]
5. Damians, I.P.; Bathurst, R.J.; Adroguer, E.A.; Josa, A.; Lloret, A. Environmental assessment of earth retaining wall structures. *Environ. Geotech.* **2017**, *4*, 415–431. [[CrossRef](#)]
6. Damians, I.P.; Bathurst, R.J.; Adroguer, E.A.; Josa, A.; Lloret, A. Sustainability assessment of earth-retaining wall structures. *Environ. Geotech.* **2018**, *5*, 187–203. [[CrossRef](#)]
7. Dixon, N.; Fowmes, G.; Frost, M. Global challenges, geosynthetic solutions and counting carbon. *Geosynth. Int.* **2017**, *24*, 451–464. [[CrossRef](#)]
8. Santos, E.C.G.; Palmeira, E.M.; Bathurst, R. Behaviour of a geogrid reinforced wall built with recycled construction and demolition waste backfill on a collapsible foundation. *Geotext. Geomembr.* **2013**, *39*, 9–19. [[CrossRef](#)]
9. Santos, E.C.G.; Palmeira, E.M.; Bathurst, R. Performance of two geosynthetic reinforced walls with recycled construction waste backfill and constructed on collapsible ground. *Geosynth. Int.* **2014**, *21*, 256–269. [[CrossRef](#)]
10. Arulrajah, A.; Rahman, M.A.; Piratheepan, J.; Bo, M.W.; Imteaz, M.A. Evaluation of interface shear strength properties of geogrid-reinforced construction and demolition materials using a modified large scale direct shear testing apparatus. *J. Mater. Civ. Eng.* **2014**, *26*, 974–982. [[CrossRef](#)]
11. Vieira, C.S.; Pereira, P.M. Interface shear properties of geosynthetics and construction and demolition waste from large-scale direct shear tests. *Geosynth. Int.* **2016**, *23*, 62–70. [[CrossRef](#)]
12. Soleimanbeigi, A.; Tanyu, B.F.; Aydilek, A.H.; Florio, P.; Abbaspour, A.; Dayioglu, A.Y.; Likos, W.J. Evaluation of recycled concrete aggregate as backfill for geosynthetic-reinforced MSE walls. *Geosynth. Int.* **2019**, *26*, 396–412. [[CrossRef](#)]
13. *ASTM D 6637*; Standard Test Method for Determining Tensile Properties of Geogrids by the Single or Multi-Rib Tensile Method. American Society for Testing and Materials: West Conshohocken, PA, USA, 2015.
14. *ASTM D4595*; Standard Test Method for Tensile Properties of Geotextiles by the Wide-Width Strip Method. American Society for Testing and Materials: West Conshohocken, PA, USA, 2017.
15. *BSI EN ISO 10319*; Geosynthetics—Wide-Width Tensile Test. British Standard Institution: London, UK, 2015.
16. *BSI 8006-1*; Code of Practice for Strengthened/Reinforced Soils and Other Fills. British Standard Institution: London, UK, 2010.
17. Allen, T.M.; Bathurst, R.J. Combined allowable strength reduction factor for geosynthetic creep and installation damage. *Geosynth. Int.* **1996**, *3*, 407–439. [[CrossRef](#)]
18. Berg, R.R.; Christopher, B.R.; Samtani, N.C. *Design of Mechanically Stabilized Earth Walls and Reinforced Soil Slopes—Volume I*; Report No. FHWA-NHI-10-024; US Department of Transportation Federal Highway Administration (FHWA): Washington, DC, USA, 2009.
19. Austin, R. The effect of installation activities and fire exposure on geogrid performance. *Geotext. Geomembr.* **1997**, *15*, 367–376. [[CrossRef](#)]
20. Richardson, G. Field evaluation of geosynthetic survivability in aggregate road base. *Geotech. Fabr. Rep.* **1998**, *16*, 34–38.
21. Hufenus, R.; Rügger, R.; Flum, D.; Sterba, I. Strength reduction factors due to installation damage of reinforcing geosynthetics. *Geotext. Geomembr.* **2005**, *23*, 401–424. [[CrossRef](#)]
22. Lim, S.Y.; McCartney, J.S. Evaluation of effect of backfill particle size on installation damage reduction factors for geogrids. *Geosynth. Int.* **2013**, *20*, 62–72. [[CrossRef](#)]
23. Pinho-Lopes, M.; Lopes, M.L. Tensile properties of geosynthetics after installation damage. *Environ. Geotech.* **2014**, *1*, 161–178. [[CrossRef](#)]
24. Pinho-Lopes, M.; Paula, A.M.; Lopes, M.L. Long-term response and design of two geosynthetics: Effect of field installation damage. *Geosynth. Int.* **2018**, *25*, 98–117. [[CrossRef](#)]
25. Santos, E.C.G.; Bueno, B.S.; Palmeira, E.M. Strength reduction of geosynthetics used in RSW built with RCDW as backfill material. In Proceedings of the 5th European Conference on Geosynthetics, Valencia, Spain, 16–19 September 2012; pp. 481–485.
26. Barbosa, F.A.S.; Santos, E.C.G. Geogrid mechanical damages due to recycled construction and demolition wastes. In Proceedings of the 14th International Waste Management and Landfill Symposium, S. Margherita di Pula, Cagliari, Italy, 30 September–4 October 2013.
27. Vieira, C.S.; Pereira, P.M. Damage induced by recycled construction and demolition wastes on the short-term tensile behaviour of two geosynthetics. *Transp. Geotech.* **2015**, *4*, 64–75. [[CrossRef](#)]
28. Barbosa, F.A.S.; Silva, E.M.; Santos, E.C.G. Polypropylene (PP) geosynthetics strength reduction due installation damages caused by construction and demolition waste (RCDW) (In Portuguese). In Proceedings of the 16th Brazilian Conference of Soils Mechanics and Geotechnical Engineering, Belo Horizonte, Brazil, 19–22 October 2016.

29. Fleury, M.P.; Santos, E.C.G.; Lins da Silva, J.; Palmeira, E.M. Geogrid installation damage caused by recycled construction and demolition waste. *Geosynth. Int.* **2019**, *26*, 641–656. [[CrossRef](#)]
30. Greenwood, J.H. The creep of geotextiles. In Proceedings of the 4th International Conference on Geotextile, Geomembranes and Related Products, Hauge, The Netherlands, 28 May–1 June 1990; pp. 645–650.
31. Greenwood, J.H. Designing to residual strength of geosynthetics instead of stress-rupture. *Geosynth. Int.* **1997**, *4*, 1–10. [[CrossRef](#)]
32. Ashmawy, A.K.; Bourdeau, P.L. Response of a woven and a nonwoven geotextile to monotonic and cyclic simple tension. *Geosynth. Int.* **1996**, *3*, 493–515. [[CrossRef](#)]
33. Bueno, B.S.; Costanzi, M.A.; Zornberg, J.G. Conventional and accelerated creep tests on nonwoven needle-punched geotextiles. *Geosynth. Int.* **2005**, *12*, 276–287. [[CrossRef](#)]
34. Chantachot, T.; Kongkitkul, W.; Tatsuoka, F. Effects of temperature rise on load-strain-time behaviour of geogrids and simulations. *Geosynth. Int.* **2018**, *25*, 287–303. [[CrossRef](#)]
35. McGown, A.; Praine, N.; Dubois, D.; Andrawes, K.Z.; Jewell, R.A. Use of geogrid properties in limit equilibrium analysis. In *Polymer Grid Reinforcement*, 1st ed.; Thomas Telford Limited: London, UK, 1985; pp. 31–36.
36. Andrawes, K.Z.; McGown, A.; Kabir, M.H. Uniaxial strength testing of woven and nonwoven geotextiles. *Geotext. Geomembr.* **1984**, *1*, 41–56. [[CrossRef](#)]
37. Wu, J.T.H.; Helwany, S.M.B. A performance test for assessment of long-term creep behavior of soil-geosynthetic composites. *Geosynth. Int.* **1996**, *3*, 107–124. [[CrossRef](#)]
38. França, F.A.N.; Bueno, B.S. Creep behavior of geosynthetics using confined-accelerated tests. *Geosynth. Int.* **2011**, *18*, 242–254. [[CrossRef](#)]
39. Zhang, Z. Experimental study on the influence of temperature and confined load on the creep characteristics of geogrid. *Adv. Mater. Res.* **2014**, *912–914*, 1629–1632. [[CrossRef](#)]
40. Zhang, Z.; Zhu, D.Y.; Chen, T.F.; Wang, T. Confined-accelerated creep tests to determine the creep reduction factor. *Appl. Mech. Mater.* **2014**, *539*, 769–773. [[CrossRef](#)]
41. Bathurst, R.J.; Huang, B.; Allen, T.M. Analysis of installation damage tests for LRFD calibration of reinforced soil structures. *Geotext. Geomembr.* **2011**, *29*, 323–334. [[CrossRef](#)]
42. Miyata, Y.; Bathurst, R.J. Reliability analysis of geogrid installation damage test data in Japan. *Soils Found.* **2015**, *55*, 393–403. [[CrossRef](#)]
43. Bathurst, R.J.; Huang, B.Q.; Allen, T.M. Interpretation of laboratory creep testing for reliability-based analysis and load and resistance factor design (LRFD) calibration. *Geosynth. Int.* **2012**, *19*, 39–53. [[CrossRef](#)]
44. Hsuan, Y.G.; Schroeder, H.F.; Rowe, R.K.; Muller, W.; Greenwood, J.; Cazzuffi, D.; Koerner, R.M. Long-term performance and lifetime prediction of the geosynthetics. In Proceedings of the 4th European Geosynthetics Conference—EuroGeo 4, Edinburgh, UK, 7–10 September 2008.
45. Kay, D.; Blond, E.; Mlynarek, J. Geosynthetics durability: A polymer chemistry issue. In Proceedings of the 57th Canadian Geotechnical Conference, Quebec City, QC, Canada, 24–27 October 2004.
46. Ionescu, A.; Kiss, S.; Dragan-Bularda, M.; Radulescu, D.; Kolozski, E.; Pintea, H.; Crisan, R. Methods used for testing the bio-colmatation and degradation of geotextiles manufactured in Romania. In Proceedings of the 2nd International Conference on Geotextiles, Las Vegas, NV, USA, 1–6 August 1982; Volume 2.
47. Yoo, H.; Jeon, H.-Y.; Chang, Y.-Y. Evaluation of engineering properties of geogrids for soil retaining walls. *Text. Res. J.* **2010**, *80*, 184–192. [[CrossRef](#)]
48. Segrestin, P.; Jailoux, J.M. Temperature in soils and its effect on the ageing of synthetic materials. *Geotext. Geomembr.* **1988**, *7*, 51–69. [[CrossRef](#)]
49. Carneiro, J.R.; Almeida, P.J.; Lopes, M.L. Some synergisms in laboratory degradation of a polypropylene geotextile. *Constr. Build. Mater.* **2014**, *73*, 586–591. [[CrossRef](#)]
50. Greenwood, J.H.; Schroeder, H.F.; Voskamp, W. *Durability of Geosynthetics*, 1st ed.; CRC Press: Boca Raton, FL, USA, 2012; p. 352, ISBN 978-90-5367-599-1.
51. Akers, S.A.S.; Studinka, J.B.; Meier, P.; Dobbt, M.G.; Johnson, D.J.; Hisaka, J. Long term durability of PVA reinforcing fibres in a cement matrix. *Int. J. Cem. Compos. Lightweight Concr.* **1989**, *11*, 79–91. [[CrossRef](#)]
52. Nishiyama, M.; Yamamoto, R.; Hoshiro, H. Long-term durability of Kuralon (PVA fiber) in alkaline condition. In Proceedings of the 10th International Inorganic-Bonded Fiber Composites Conference—IBCC, São Paulo, Brazil, 15–18 November 2006; pp. 120–134.
53. Petrik, P.M.; Baslák, R. Design of geotextiles reinforcing embankments with reference to long-term loading. *Geotext. Geomembr.* **1988**, *7*, 71–89. [[CrossRef](#)]
54. Jailoux, J.-M.; Nait-Ali, K.L.; Freitag, N. Exhaustive long-term study on hydrolysis of high-tenacity polyester—10 year results. In Proceedings of the 4th European Geosynthetics Conference—EuroGeo 4, Edinburgh, UK, 7–10 September 2008; p. 6.
55. Crawford, R.J. *Plastics Engineering*, 3rd ed.; Butterworth-Heinemann Press: Oxford, UK, 1998; p. 352. ISBN 978-07-5063-764-0.
56. Halse, Y.; Koerner, R.M.; Lord, A.E., Jr. Effect of high levels of alkalinity on geotextiles. Part 1: Ca(OH)₂ Solutions. *Geotext. Geomembr.* **1987**, *5*, 261–282. [[CrossRef](#)]
57. Elias, V.; Salman, A.; Goulias, D. The effect of pH, resin properties, and manufacturing process on laboratory degradation of polyester geosynthetics. *Geosynth. Int.* **1998**, *5*, 459–490. [[CrossRef](#)]

58. Burgoyne, C.J.; Merri, A.L. On the hydrolytic stability of polyester yarns. *J. Mater. Sci.* **2007**, *42*, 2867–2878. [[CrossRef](#)]
59. Duvall, D.E. Impact of product structure on the stability and durability of coated poly(ethylene terephthalate) geogrids. *Geotext. Geomembr.* **1994**, *13*, 133–145. [[CrossRef](#)]
60. Al-awadhi, J.M. Impact of gravel quarrying on the desert environment of Kuwait. *Environ. Earth Sci.* **2001**, *41*, 365–371. [[CrossRef](#)]
61. Azam, A.M.; Cameron, D.A. Laboratory evaluation of recycled concrete aggregate and recycled clay masonry blends in pavement applications. *Adv. Civ. Eng. Mater.* **2013**, *2*, 20120016. [[CrossRef](#)]
62. O'Mahony, M.M. An analysis of the shear strength of recycled aggregates. *Mater. Struct.* **1997**, *30*, 599–606. [[CrossRef](#)]
63. Garg, N.; Thompson, M. Lincoln Avenue reclaimed asphalt pavement base project. *Transp. Res. Rec.* **1996**, *1547*, 89–95. [[CrossRef](#)]
64. Aqil, U.; Tatsuoka, F.; Uchimura, T. Strength and deformation characteristics of recycled concrete aggregate in triaxial compression. In *GSP 138 Site Characterization and Modelling*; American Society of Civil Engineers: Reston, VA, USA, 2005; 10p. [[CrossRef](#)]
65. Kang, D.-H.; Gupta, S.C.; Ranaivoson, A.Z.; Siekmeier, J.; Roberson, R. Recycled materials as substitutes for virgin aggregates in road construction: I. Hydraulic and mechanical characteristics. *Soil Sci. Soc. Am. J.* **2011**, *75*, 1265–1275. [[CrossRef](#)]
66. Arulrajah, A.; Piratheepan, J.; Ali, M.M.Y.; Bo, M.W. Geotechnical properties of recycled concrete aggregate in pavement sub-base applications. *Geotech. Test. J.* **2012**, *35*, 743–751. [[CrossRef](#)]
67. Cameron, D.A.; Azam, A.H.; Rahman, M.M. Recycled clay masonry and recycled concrete aggregate blends in pavement. In Proceedings of the GeoCongress 2012, Oakland, CA, USA, 25–29 March 2012; p. 10.
68. Delongui, L.; Matuella, M.; Núñez, W.P.; Fedrigo, W.; da Silva Filho, L.C.P.; Ceratti, J.A.P. Construction and demolition waste parameters for rational pavement design. *Constr. Build. Mater.* **2018**, *168*, 105–112. [[CrossRef](#)]
69. Bennert, T.; Papp, W.J.; Maher, A.; Gucunski, N. Utilization of construction and demolition debris under traffic-type loading in base and subbase applications. *Transp. Res. Board* **2000**, *1714*, 33–39. [[CrossRef](#)]
70. Santos, E.C.G.; Vilar, O.M. Use of recycled construction and demolition wastes (RCDW) as backfill of reinforced soil structures. In Proceedings of the 4th European Geosynthetics Conference—EuroGeo 4, Edinburgh, UK, 7–10 September 2008; p. 8.
71. Vieira, C.S.; Pereira, P.M.; Lopes, M.L. Recycled construction and demolition wastes as filling material for geosynthetic reinforced structures. Interface properties. *J. Clean. Prod.* **2016**, *124*, 299–311. [[CrossRef](#)]
72. Vieira, C.S. Valorization of fine-grain construction and demolition (c&d) waste in geosynthetic reinforced structures. *Waste Biomass Valorization* **2018**, *4*, 1615–1626. [[CrossRef](#)]
73. Soleimanbeiji, A.; Likos, W. Mechanical properties of recycled concrete aggregate and recycled asphalt pavement reinforced with geosynthetics. In Proceedings of the Geo-Congress 2019, Philadelphia, PA, USA, 24–27 March 2019; p. 9.
74. Touahamia, M.; Sivakumar, V.; McKelvey, D. Shear strength of reinforced-recycled material. *Constr. Build. Mater.* **2002**, *16*, 331–339. [[CrossRef](#)]
75. Vieira, C.S.; Ferreira, F.B.; Pereira, P.M.; Lopes, M.L. Pullout behaviour of geosynthetics in a recycled construction and demolition material—Effects of cyclic loading. *Transp. Geotech.* **2020**, *23*, 100346. [[CrossRef](#)]
76. Santos, E.C.G.; Palmeira, E.M.; Bathurst, R. Construction of a full-scale wrapped face geogrid reinforced wall using recycled construction and demolition waste as backfill material. In Proceedings of the 9th International Conference on Geosynthetics, Guarujá, Brazil, 23–27 May 2010; Palmeira, E.M., Vidal, D.M., Sayão, A.S.J.F., Ehrlich, M., Eds.; International Geosynthetic Society (Chapter Brazil): Guarujá, Brazil, 2010; pp. 1769–1772.
77. Ulsen, C.; Kahn, H.; Angulo, S.C.; John, V.M. Chemical composition of mixed construction and demolition recycled aggregates from the State of São Paulo. *Rev. Esc. Minas* **2010**, *63*, 339–346. [[CrossRef](#)]
78. Rambaldi, E.; Esposito, L.; Tucci, A.; Timellini, G. Recycling of polish porcelain stoneware residues in ceramic tiles. *J. Eur. Ceram. Soc.* **2007**, *27*, 3509–3515. [[CrossRef](#)]
79. Bernardin, A.M.; Silva, M.J.; Riella, H.G. Characterization of cellular ceramics made by porcelain tile residues. *Mater. Sci. Eng. A.* **2006**, *437*, 222–225. [[CrossRef](#)]
80. Pacheco-Torgal, F.; Jalali, S. Reusing ceramic wastes in concrete. *Constr. Build. Mater.* **2010**, *24*, 832–838. [[CrossRef](#)]
81. Barbudo, A.; Galvín, A.P.; Agrela, F.; Ayuso, J.; Jiménez, J.R. Correlation analysis between sulphate content and leaching of sulphates in recycled aggregates from construction and demolition wastes. *Waste Manag.* **2012**, *32*, 1229–1335. [[CrossRef](#)]
82. Ferreira, F.B.; Pereira, P.; Vieira, C.S. Long-term tensile behavior of a high-strength geotextile after exposure to recycled construction and demolition material. *J. Mater. Civ. Eng.* **2022**, *34*, 04022046. [[CrossRef](#)]
83. Stook, K.; Tolaymat, T.; Ward, M.; Dubey, B.; Townsend, T.; Solo-Gabriele, H.; Bitton, G. Relative leaching and aquatic toxicity of pressure-treated wood products using batch leaching tests. *Environ. Sci. Technol.* **2005**, *39*, 155–163. [[CrossRef](#)]
84. Asakura, H. Sulfate and organic matter concentration in relation to hydrogen sulfide generation at inert solid waste landfill site—Limit value for gypsum. *Waste Manag.* **2015**, *43*, 328–334. [[CrossRef](#)]
85. Asakura, H.; Watanabe, Y.; Ono, Y.; Yamada, M.; Inoue, Y.; Alfaro, A.M. Characteristics of fine processed construction and demolition waste in Japan and method to obtain fines having low gypsum component and wood contents. *Waste Manag. Res.* **2009**, *28*, 634–646. [[CrossRef](#)] [[PubMed](#)]
86. Townsend, T.G.; Jang, Y.; Thurn, L.G. Simulation of construction and demolition waste leachate. *J. Environ. Eng.* **1999**, *125*, 1071–1081. [[CrossRef](#)]
87. Lee, S.; Xu, Q.; Townsend, T.G.; Chadik, P.; Bitton, G. Reduced sulfur compounds in gas from construction and demolition debris landfills. *Waste Manag.* **2006**, *26*, 526–533. [[CrossRef](#)] [[PubMed](#)]

88. Xu, Q.; Townsend, T. Factors affecting temporal H₂S emission at construction and demolition (C&D) debris landfills. *Chemosphere* **2014**, *96*, 105–111. [[CrossRef](#)] [[PubMed](#)]
89. Arulrajah, A.; Piratheepan, J.; Disfani, M.; Bo, M. Geotechnical and geoenvironmental properties of recycled construction and demolition materials in pavement subbase applications. *J. Mater. Civ. Eng.* **2013**, *25*, 1077–1088. [[CrossRef](#)]
90. Collares, A.C.Z.B.; Vilar, O.M. The influence of some chemical properties of soaking liquids on the collapse of tropical soils. In Proceedings of the Second Pan-American Conference on Unsaturated Soils, Dallas, TX, USA, 12–15 November 2017; Volume 1, p. 10.
91. Lafiti, N.; Eisazadeh, A.; Marto, A.; Meehan, C.L. Tropical residual soil stabilization: A powder form material for increasing soil strength. *Constr. Build. Mater.* **2017**, *147*, 827–883. [[CrossRef](#)]
92. Lopes, A.S.; Guilherme, L.R.G. A career perspective on soil management in the Cerrado Region of Brazil. *Adv. Agron.* **2016**, *137*, 1–72. [[CrossRef](#)]
93. Lima, A.S.; Cabral, A.E.B. Characterization and classification of construction waste in Fortaleza (CE). *Eng. Sanit. Ambient.* **2013**, *18*, 169–176. [[CrossRef](#)]
94. Coelho, E.E.; Pereira, L.A.; Nozaki, N.K.S.; Pasqualetto, A. Evaluation of rain-water acidity in the municipality of Goiânia-GO. In *Gestão das Águas*; Pasqualetto, A., Ed.; Editora da UCG: Goiânia, GO, Brazil, 2005; pp. 109–120. ISBN 857103229-7. (In Portuguese)
95. USEPA 9045D; Soil and Waste pH. Test Methods for Evaluating Solid Waste, Physical/Chemical Methods (SW846). United States Environmental Protection Agency: Washington, DC, USA, 2004.
96. Santos, E.C.G. Application of Recycled Construction and Demolition Waste (RCDW) in Reinforced Soil Structures. Master's Thesis, University of São Paulo, São Carlos, Brazil, 2007. (In Portuguese)
97. Leite, F.C.; Motta, R.S.; Vasconcelos, K.L.; Bernucci, L. Laboratory evaluation of recycled construction and demolition waste for pavements. *Constr. Build. Mater.* **2011**, *25*, 2972–2979. [[CrossRef](#)]
98. CONAMA. *Resolution 307*; Brazilian National Environment National Council: Brasília, Brazil, 2003. (In Portuguese)
99. NCMA. *Design Manual for Segmental Retaining Walls*, 3rd ed.; National Concrete Masonry Association: Herndon, VA, USA, 2010.
100. FHWA. *Design and Construction of Mechanically Stabilized Earth Walls and Reinforced Soil Slopes*; Berg, R.R., Christopher, B.R., Samtani, N.C., Eds.; FHWA-NHI-10-024; Federal Highway Administration: Washington, DC, USA, 2010.
101. ASTM D2487-17E1; Standard Practice for Classification of Soils for Engineering Purposes (Unified Soil Classification System). American Society for Testing and Materials: West Conshohocken, PA, USA, 2006.
102. EBGeo. *Recommendations for Design and Analysis of Earth Structures Using Geosynthetic Reinforcements—EBGeo*; German Geotechnical Society, Ernst and Sohn GmbH & Co. KG: Berlin, Germany, 2011.
103. ABNT NBR 10004; Solid Waste: Classification. Brazilian Association of Technical Standards: Rio de Janeiro, Brazil, 2004. (In Portuguese)
104. ASTM D7748M-14; Standard Test Method for Flexural Rigidity of Geogrids, Geotextiles, and Related Products. American Society for Testing and Materials: West Conshohocken, PA, USA, 2021.

Disclaimer/Publisher's Note: The statements, opinions and data contained in all publications are solely those of the individual author(s) and contributor(s) and not of MDPI and/or the editor(s). MDPI and/or the editor(s) disclaim responsibility for any injury to people or property resulting from any ideas, methods, instructions or products referred to in the content.